Received: 21 November 2017 | Revised: 14 April 2018 | Accepted: 16 April 2018

DOI: 10.1111/pce.13322

ORIGINAL ARTICLE

WILEY Plant, Cell & Environment

Water transport through tall trees: A vertically explicit, analytical model of xylem hydraulic conductance in stems

Valentin Couvreur[1] | Glenn Ledder[2] | Stefano Manzoni[3] | Danielle A. Way[4,5] | Erik B. Muller[6,7] | Sabrina E. Russo[8]

[1] Earth and Life Institute—Agronomy, Université Catholique de Louvain, Louvain-la-Neuve, Belgium

[2] Department of Mathematics, University of Nebraska—Lincoln, Lincoln, NE, USA

[3] Department of Physical Geography and Bolin Centre for Climate Research, Stockholm University, Stockholm, Sweden

[4] Department of Biology, University of Western Ontario, London, Ontario N6A 5B7, Canada

[5] Nicholas School of the Environment, Duke University, Durham, NC 27708, USA

[6] Department of Biology, Norwegian University of Science and Technology, Trondheim, Norway

[7] Marine Science Institute, University of California, Santa Barbara, CA, USA

[8] School of Biological Sciences, University of Nebraska—Lincoln, Lincoln, NE, USA

Correspondence
S. E. Russo, School of Biological Sciences, University of Nebraska—Lincoln, Lincoln, NE, USA.
Email: srusso2@unl.edu

Funding information
"Fonds Spéciaux de Recherche" (FSR) of the Université Catholique de Louvain; Wallonie-Bruxelles International; Belgian American Educational Foundation; Communauté française de Belgique-Actions de Recherches Concertées, Grant/Award Number: ARC16/21-075; Interuniversity Attraction Poles Programme—Belgian Science Policy, Grant/Award Number: IAP7/29; Ontario Early Career Award; Canadian Natural Sciences and Engineering Research Council; NIMBIOS; Swedish Research Council Formas, Grant/Award Number: 2016-00998; UNL College of Arts and Sciences International Research Collaborations Award; National Science Foundation, Grant/Award Number: DBI-1300426

Abstract

Trees grow by vertically extending their stems, so accurate stem hydraulic models are fundamental to understanding the hydraulic challenges faced by tall trees. Using a literature survey, we showed that many tree species exhibit continuous vertical variation in hydraulic traits. To examine the effects of this variation on hydraulic function, we developed a spatially explicit, analytical water transport model for stems. Our model allows Huber ratio, stem-saturated conductivity, pressure at 50% loss of conductivity, leaf area, and transpiration rate to vary continuously along the hydraulic path. Predictions from our model differ from a matric flux potential model parameterized with uniform traits. Analyses show that cavitation is a whole-stem emergent property resulting from non-linear pressure-conductivity feedbacks that, with gravity, cause impaired water transport to accumulate along the path. Because of the compounding effects of vertical trait variation on hydraulic function, growing proportionally more sapwood and building tapered xylem with height, as well as reducing xylem vulnerability only at branch tips while maintaining transport capacity at the stem base, can compensate for these effects. We therefore conclude that the adaptive significance of vertical variation in stem hydraulic traits is to allow trees to grow tall and tolerate operating near their hydraulic limits.

KEYWORDS

gravity, Huber ratio, matric flux potential, sapwood saturated conductivity, tree height, water relations, xylem cavitation, xylem transport

1 | INTRODUCTION

Tall trees play critical roles in structuring forest communities and storing carbon (Lindenmayer & Laurance, 2017; Lutz, Larson, Swanson, & Freund, 2012) and comprise a large proportion of the living biomass in the world's forests (Lutz, Larson, Freund, Swanson, & Bible, 2013; Slik et al., 2013; Stephenson et al., 2014). As Earth's climate regimes continue to shift, changes in the growth and survival of tall trees are

anticipated to have disproportionately large effects on global biogeochemical cycles (Martin et al., 2001; Rifai et al., 2016; Slik et al., 2013). This is because, compared with shorter trees, taller trees have different water use patterns (Brienen et al., 2017; Koch, Sillett, Jennings, & Davis, 2004; Warren & Adams, 2000) and are often found to be more vulnerable to drought (Bennett, McDowell, Allen, & Anderson-Teixeira, 2015; Mueller et al., 2005; Nepstad, Tohver, Ray, Moutinho, & Cardinot, 2007; Prior & Bowman, 2014; Rowland et al., 2015), partly due to the challenges associated with raising water to tall heights (Mohr & Schopfer, 1995). Trees grow tall by vertical extension of the stem with hydraulic traits adjusted to height, and so accurate, mechanistic hydraulic models for water flow in stems are fundamental to understanding the hydraulic challenges faced by tall trees.

Water transport through xylem is critical for sustaining canopy gas exchange and cell expansion, and, hence, for plant growth and survival. Water flow occurs under tension as water moves from less negative ψ in the soil and roots to more negative values in leaves (Tyree & Ewers, 1991). In short plants, in which gravitational effects are negligible, water potential (ψ) is approximately equal to xylem pressure (P), which decreases along the xylem system due to frictional pressure losses as water moves through the xylem conduits. Depending on the species and growing conditions, this gradient in P can be as high as −0.1 MPa/m (Cruiziat, Cochard, & Ameglio, 2002). Although steeper gradients of P can be found in roots and leaves, the gradients in P in the stem interact with the pressures in these organs and therefore affect hydraulic functioning of the whole plant system. The pressure loss equals the ratio of the water flow rate to the conductance of the xylem conduits, which approximately scales with the fourth power of their radius (Sanderson, Whitbread, & Clarkson, 1988). Hence, steeper gradients in xylem P are expected in narrower xylem elements and under high transpiration rates, but also when there are fewer conduits. The hydrostatic pressure gradient driven by gravity (or specific weight of water, 9.81×10^{-3} MPa/m) also contributes to the reduction in P upwards from the ground. As plants grow taller, the contribution of gravity becomes increasingly important relative to frictional pressure losses and eventually limits maximum plant height (Ambrose, Sillett, & Dawson, 2009; Koch et al., 2004).

The decline in P with higher vertical position along the xylem path and with faster water flow has two main consequences. First, more negative P triggers stomatal closure (Lawlor & Tezara, 2009), a negative feedback that limits further decreases in P by reducing transpiration from leaves. Second, more negative P causes cavitation and air embolism (Cruiziat et al., 2002), which decrease the hydraulic conductivity of the xylem, impairing water transport capacity (Tyree & Sperry, 1989). To compensate for height- and friction-related decreases in P, xylem conduits taper from the roots towards the distal parts of the canopy (McCulloh, Sperry, & Adler, 2003; Olson et al., 2014; Savage et al., 2010). This strategy allows for "efficient" transport in the lower part of the stem, where conduits are wide and P is less negative, and "safer" transport in more distal parts, where P is more negative but conduits are narrower and more resistant to hydraulic damage (Johnson et al., 2016).

Height-dependent hydraulic traits determine sapwood conductive properties, which interact with gravity- and transport-driven P gradients to create clear vertical profiles of P that constrain virtually all plant ecophysiological processes (Burgess, Pittermann, & Dawson, 2006; Givnish, Wong, Stuart-Williams, Holloway-Phillips, & Farquhar, 2014; McCulloh et al., 2003). Xylem anatomy governs intrinsic hydraulic traits, such as saturated sapwood conductivity and water potential at 50% loss of conductivity. Even within stems, these traits can exhibit substantial variation both vertically within a tree and among trees of different heights (Ambrose et al., 2009; Delzon, Sartore, Burlett, Dewar, & Loustau, 2004; Domec, Lachenbruch, Pruyn, & Spicer, 2012; Johnson et al., 2016; McCulloh, Johnson, Meinzer, & Woodruff, 2014; Zaehle, 2005; Zhang et al., 2009; Zimmerman, 1983). Water transport depends on not only these intrinsic traits but also extrinsic traits that are determined by allocation, tree geometry, and size. In particular, the leaf-to-sapwood area ratio (also called the Huber ratio) modulates the relative importance of evaporative demand and water supply through the xylem and varies within stems depending on vertical position and tree height (Bohrer et al., 2005; Burgess et al., 2006; Delzon et al., 2004; Huber, 1928; McDowell et al., 2002; Novick et al., 2009; Zhang et al., 2009).

Because vertical profiles in P are crucial for plant function, it is important for plant physiological and hydrologic models to capture their physical and biological drivers, including vertical variation in hydraulic traits in stems. Darcy's law, which describes fluid flow through a porous medium (Darcy, 1856), is a starting point for plant hydraulic models describing the relationship between bulk flow of water through saturated sapwood and the P gradient driving flow. However, Darcy's law does not account for water storage, which can be important in trees (Čermák, Kučera, Bauerle, Phillips, & Hinckley, 2007; Matheny et al., 2015; Scholz et al., 2007), and so must be generalized to Richards' equation (Richards, 1931) if variation in storage is to be included. At least three major classes of models address vertical profiles in P to some extent. We will refer to them as discrete models, matric flux potential (MFP) models, and continuous models. These models differ with regard to how vertical variation in hydraulic traits and in the realized sapwood conductivity (k) and P are modelled (Comstock & Sperry, 2000). In discrete models (e.g., Christoffersen et al., 2016; Manzoni et al., 2013; Manzoni, Katul, & Porporato, 2014; Mencuccini, Minunno, Salmon, Martínez-Vilalta, & Hölttä, 2015; Novick et al., 2009; Tyree & Sperry, 1988; van den Honert, 1948), the continuous hydraulic path is divided into discrete segments, the hydraulic traits of which are assumed to be uniform. For each segment, k is calculated from the values of P at the nodal ends (e.g., the average of the values of P). As a result, the spatially continuous relationship between k and P along the hydraulic path is approximated, and the pressure–flow relation along each segment of finite size is linearized. This approach is problematic because the negative feedback of continuous water tension on xylem conductivity generates substantial non-linearity in the pressure–flow relation, and this non-linearity is not accounted for within segments in discrete models (Comstock & Sperry, 2000). These approximations can systematically overestimate or underestimate the extent of cavitation when xylem vulnerability or other hydraulic traits vary vertically within a stem (Figure 1). Finer segmentation of the hydraulic path reduces the inaccuracies of these approximations in discrete models (Mencuccini et al., 2015), but at the cost of considerable increases in computational time (Meunier, Draye, Vanderborght, Javaux, & Couvreur, 2017).

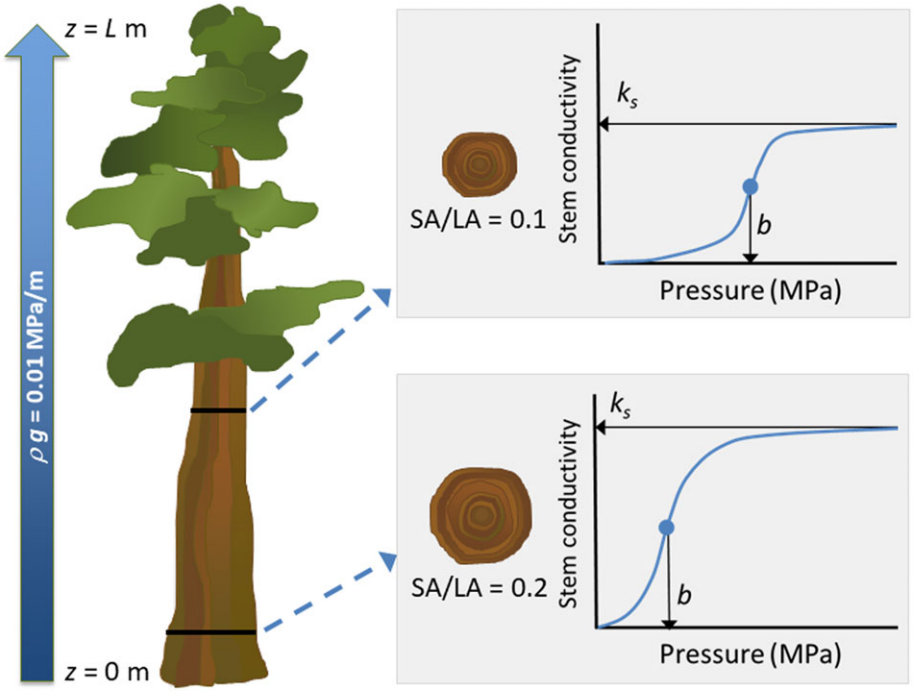

FIGURE 1 Conceptual figure showing how hydraulic traits may change with height within a tree. The height along a tree stem (z) goes from zero at ground level to L, the total hydraulic path length (corresponding to tree height H), and here, we depict changes in hydraulic traits for two exemplary values of z, closer to the base versus the top of the tree. The Huber value (h, the ratio of sapwood area to leaf area) is often observed to be greater at the base of the tree than at taller heights up the tree. Likewise, the shape of the xylem vulnerability curve, describing variation in stem conductivity with xylem pressure, also changes with height in the tree due to changes in the pressure, at which 50% of the stem conductivity is lost (b) and the stem-saturated hydraulic conductivity (k_s), both of which have been observed to increase with z. Gravitational potential increases 0.01 MPa for every meter of tree height, which contributes to reductions in the water potential at taller tree heights [Colour figure can be viewed at wileyonlinelibrary.com]

MFP models (e.g., Loranty, Mackay, Ewers, Traver, & Kruger, 2010; Mackay et al., 2015; Sperry, Adler, Campbell, & Comstock, 1998; Sperry et al., 2016; Wolf, Anderegg, & Pacala, 2016) improve upon discrete models by integrating the pressure–conductivity relation over the range of pressures that occur in each segment. Hence, MFP models neither approximate the k–P feedback nor linearize the k–P relationship within a segment (Comstock & Sperry, 2000). However, MFP models are not spatially explicit because they can only predict k or P at nodes between segments, not at any point within a segment. Furthermore, the fact that MFP models integrate a single vulnerability curve over P allows for continuous within-segment variation in k, but not in intrinsic traits (e.g., saturated conductivity, P_{50}), extrinsic traits (e.g., sapwood area), nor gravity. Variation in hydraulic traits and the effect of gravity can therefore only be accounted for discretely from one segment to the next.

Continuous models (e.g., Aumann & Ford, 2002; Bohrer et al., 2005; Chuang, Oren, Bertozzi, Phillips, & Katul, 2006; Mirfenderesgi et al., 2016) begin with either the pointwise Darcy's law (if neglecting variation in water storage) or Richards' equation (if including it). They treat position along the hydraulic path as a continuous variable, explicitly represent the non-linear k–P feedback, and yield continuous P profiles without requiring any segmentation. In principle, hydraulic traits (both extrinsic and intrinsic) can also vary continuously along the hydraulic path in continuous models. This has been implemented for sapwood area (Bohrer et al., 2005; Chuang et al., 2006; Mirfenderesgi et al., 2016). However, variation in intrinsic hydraulic traits has not, to our knowledge, been implemented in any model.

We present a spatially explicit, analytical water transport model for tree stems that generalizes existing models so as to allow continuous vertical variation in transpiration, gravity, and the intrinsic and extrinsic hydraulic traits governing water flow in stems. Specifically, our model allows the Huber ratio, the stem-saturated conductivity, and pressure at 50% loss of conductivity (P_{50}) to vary as continuous functions of position along the path and allows for leaves to be distributed along the hydraulic pathway, rather than only at the top of the tree. We also derived a stem-specific formula for the theoretical maximum sustainable water flow, Q_{crit}, which is closely related to the theoretical maximum transpiration rate (E_{crit}; Tyree & Sperry, 1988; Sperry et al., 2016). Analysis of our model therefore allows a theoretical examination of the effects of continuous variation in hydraulic traits on k, P, stem hydraulic conductance (K_s), cavitation, and Q_{crit} in stems, which has not previously been done. We first describe the model, its assumptions, and scope of inference and present its mathematical derivation. Second, we analysed empirical data on vertical variation in hydraulic traits with height within a tree and among trees of different heights and develop functional forms describing this variation. Third, we evaluated the performance of our model by parameterizing it with empirical data and comparing its predicted vertical variation in k and P with observations from the same tree from which the parameter values for hydraulic traits were derived. Fourth, we theoretically examined the effects of continuous variation in hydraulic

traits on vertical profiles in k, P, and cavitation. Last, we compared the predictions of our model with a commonly used MFP approach to test whether, given a particular set of continuously varying hydraulic traits, Q_{crit}, and the predicted vertical profiles of k, P, and cavitation depend upon the modelling approach.

2 | MODEL SCOPE AND ASSUMPTIONS

Here, we summarize the scope and assumptions of our model, but these are elaborated upon in subsequent sections. (a) Our model includes a mechanistic description of the hydraulic pathway from the base of the stem to the xylem terminus in the twigs before the petioles. It is coupled to a simple, demand-driven leaf transpiration model, and we set the xylem pressure at the base of the stem and the transpiration rate per unit leaf area. Therefore, our model comprises a stem module that excludes leaf, root, and soil hydraulics and stomatal feedbacks. Accurate hydraulic models for stems are important because even though the leaf has a higher resistance than the stem, the leaf is sensitive to the pressure that comes from the stem and stem hydraulics may limit total leaf transpiration (McCulloh & Sperry, 2005; Zimmerman, 1983). Our model can easily be coupled to models of leaf hydraulics and stomatal control (e.g., Farquhar, von Caemmerer, & Berry, 1980; Sack & Holbrook, 2006) at the upper end and root and soil models (e.g., Couvreur, Vanderborght, Beff, & Javaux, 2014; de Jong van Lier, van Dam, Metselaar, de Jong, & Duijnisveld, 2008) at the lower end, to examine the soil–plant atmosphere hydraulic continuum and allow a dynamic relationship between conductivity, pressure, and transpiration rate. (b) Our model is designed to apply at the daily timescale and so does not account for changes in water storage. Water storage can be important for tall trees (Čermák et al., 2007; Matheny et al., 2015; Scholz et al., 2007) and is accounted for in some models that operate at timescales of hours or less (Bohrer et al., 2005; Christoffersen et al., 2016; Xu, Medvigy, Powers, Becknell, & Guan, 2016). Provided there are no major environmental changes (e.g., no dramatic soil drying), tree water storage recovers diurnally, and hence, the contribution of changes in storage to cumulative transpiration over a day or multiple days is negligible (e.g., Čermák et al., 2007; Phillips, Nagchaudhuri, Oren, & Katul, 1997). (c) Because the constraints on water flow in stems is our focus, our model does not include a detailed description of crown architecture and so does not require segmentation of the hydraulic path, as in previous models (e.g., FETCH; Bohrer et al., 2005). However, our model does accommodate a simple tree crown, in which the hydraulic path length can vary among branches. In our model, the values for hydraulic traits are the same at a given distance along the hydraulic path on any branch. As a result, we do not need to consider the tapering of individual branches or the trunk, because the total sapwood cross-sectional area is explicitly represented at a given point along the hydraulic path, as in the Da Vinci scaling rule (Savage et al., 2010; West, Brown, & Enquist, 1999). (d) Our model explicitly accounts for the effects of gravity when branches are vertical and uses a first-order correction of this to account for laterally spreading branches in the tree crown. (e) Despite the absence of any segmentation of the hydraulic path, our model allows the following to be provided as inputs and to vary as continuous functions of position along the hydraulic path: leaf area, transpiration per unit leaf area, and hydraulic traits (sapwood saturated conductivity, P_{50}, and Huber ratio). (f) As a result, k, P, and water flow also vary continuously and are predicted by our model for any point along the path. Our model thus has space (i.e., position on the hydraulic path) as an independent variable, but not time, and so gives an equilibrium solution that adjusts instantaneously to environmental changes. An equilibrium solution is appropriate for examining how vertical variation in hydraulic traits affects pressure profiles and the location of catastrophic cavitation. Our approach is therefore conservative, as storage changes can delay the occurrence of damage. Moreover, our model explicitly accounts for the spatially continuous nonlinear feedbacks between conductivity and pressure that determine water flow along the hydraulic pathway while allowing for continuous variation in intrinsic and extrinsic hydraulic traits. (g) Our general solution is an explicit integral formula that can be evaluated using standard numerical routines found in general mathematical software. With some additional simplifying assumptions, the solution reduces to an explicit algebraic formula. Either of these solutions would be straightforward to implement in trait-based dynamic global vegetation and earth systems models (van Bodegom, Douma, & Verheijen, 2014; Wang et al., 2017), with the fully analytical solution being of particular value when computational efficiency is important. (h) Other assumptions include that there is no significant extra-xylary water transport and that all of the water transported through stems is ultimately transpired, rather than used for other purposes, such as construction of new tissues. Below, we present an abbreviated derivation of the model, focusing on the biological assumptions and primary results, with additional details in Appendix S1. Variables, parameters, functions, and constants are defined in Table 1.

3 | MODEL DESCRIPTION

3.1 | General mathematical formulation

We first present a general formulation of our model, in which as many as possible of the properties determining the flow rate are allowed to vary along the length L of the hydraulic pathway. We couple our stem module to a leaf boundary, so that water flow is driven by a plausible transpiration rate at the leaf level, but this transpiration is set based on environmental conditions without feedback from the hydraulic system. This allows us to isolate the behaviour of the stem hydraulic system for the purpose of elucidating the limitations that the stem imposes on the functioning of the tree in its environment. The hydraulic model can also be used to determine the maximum total flow rate that can be achieved through the stem under the additional assumption that E does not vary along the hydraulic pathway (see Section 3.3).

Let $A_l(z)$ (m^2) be the total leaf area downstream from the point z (m) along the stem hydraulic path that starts at $z = 0$ and ends at $z = L$,

$$A_l(z) = A_T + \int_z^L d_l(\bar{z})\, d\bar{z}, \tag{1}$$

where A_T (m^2) is the leaf area at $z = L$ and $d_l(z)$ (m^2/m) is a leaf area density function that prescribes the distribution of leaf area along

TABLE 1 Variables, functions, parameters, and constants and conversion factors used in the model

	Description	Units
Variables		
E_{crit}	Theoretical maximum transpiration rate per unit leaf area	mmol/m^2 (leaf)-s
Q_{crit}	Theoretical maximum water flow rate through the stem	kg/s
P	Hydrostatic pressure	MPa
Y	The reciprocal of the fractional loss of conductivity at each point (fractional loss of conductivity is percent loss of conductivity/100)	dimensionless
z	Distance from the base of the tree along the hydraulic path length (assumed to be the same as vertical height)	m
ψ	Water potential	MPa
Functions		
$A_l(z)$	Total area of leaves above point z	m^2 (leaf)
$A_s(z)$	Sapwood area at point z	cm^2 (sapwood)
$b(z)$	Pressure at 50% loss of conductivity in vulnerability curve (P_{50}) at point z	MPa
$d_l(z)$	Density function for leaf area at point z	m^2 (leaf)/m (path length)
$E(z)$	Transpiration rate per unit leaf area at point z	mmol/m^2 (leaf)-s
$f(P,z)$	Vulnerability curve function	dimensionless
$h(z)$	Huber ratio (sapwood area at point z/leaf area above point z)	cm^2 (sapwood)/m^2 (leaf)
$K(P)$	Actual hydraulic conductance	kg/s-MPa
$k(P,z)$	Actual hydraulic conductivity	kg-m/m^2 (sapwood)-s-MPa
$k_s(z)$	Saturated hydraulic conductivity at point z	kg-m/m^2 (sapwood)-s-MPa
$Q(z)$	Water flow at point z	kg/s
$r(z)$	Resistance per unit path length at point z: $r = 10^4/A_s k_s$	MPa-s/kg-m
$\tilde{z}(z)$	Vertical height at point z	m
$\alpha(z)$	Adjustment factor for gravitational force	dimensionless
$\beta(z)$	Combination of P_{50} gradient and gravity at point z: $\beta = -db/dz\text{-}\rho g$	MPa/m
Parameters		
A_T	Area of leaves at $z = L$	m^2 (leaf)
a	Shape parameter of vulnerability curve	1/MPa
b_0	Pressure at 50% loss of conductivity in vulnerability curve (P_{50}) at the base of the tree ($z = 0$)	MPa
b_s	Slope parameter for change in b along the height of the tree	MPa/m
b_T	Pressure at 50% loss of conductivity in vulnerability curve (P_{50}) at the top of the tree ($z = L$)	MPa
b_1	Fitted parameter	MPa
E	Transpiration rate per unit leaf area	mmol/m^2 (leaf)-s
γ	Fixed parameter	m^{-1}
H	Tree height	m
h_0	Huber ratio (sapwood area/leaf area) at the base of the tree	cm^2 (sapwood)/m^2 (leaf)
h_s	Slope of the Huber ratio function	cm^2 (sapwood)/m^2 (leaf)-m
k_0	Stem saturated hydraulic conductivity at the base of the tree	kg-m/m^2 (sapwood)-s-MPa
k_{exp}	Shape parameter of the stem saturated hydraulic conductivity curve	dimensionless
L	Hydraulic path length	m
P_0	Pressure at the base of the tree	MPa
Y_0	Value of Y at the base of the tree	dimensionless
Z_{50}	Fraction of tree height at which the saturated hydraulic conductivity is half that at the base	dimensionless
Constants		
ρg	Specific weight of water (~0.01)	MPa/m

Note. All quantities involving mass or molar quantities refer to water (with molecular weight 0.018 kg/mol).

the hydraulic path. This formulation allows for maximum flexibility by distributing some leaves at the end of the pathway (A_T) and others below (the second term in Equation (1)).

Given the assumption that all the transported water is ultimately transpired and that changes in water storage can be neglected over timescales of more than a day, the total flow rate Q (kg/s) across the

sapwood at any point z must match the total transpiration downstream from that point,

$$Q(z) = 18\times10^{-6}\left(E(L)A_T + \int_z^L E(\bar{z})d_l(\bar{z})d(\bar{z})\right), \quad (2)$$

where E represents the transpiration rate per unit leaf area in mmol/m^2 (leaf)-s and the numerical coefficient converts mmol to kg.

Our continuous model is derived from the pointwise version of Darcy's law (Darcy, 1856)

$$\frac{Q(z)}{10^{-4}A_s(z)} = -k(P,z)\frac{d\psi}{dz}, \quad (3)$$

where the factor 10^{-4} converts units of cm^2 to m^2, A_s is the sapwood area (cm^2), and k is the xylem tissue hydraulic conductivity (kg/m-s-MPa). To Equation (3), we add the effects of both gravity and pressure on the water potential:

$$\psi = P + \rho g\tilde{z}(z), \quad (4)$$

where ρg is the specific weight of water (9.81×10^{-3} MPa/m) and $\tilde{z}(z)$ is the average vertical height among branches of the points located at position z along the hydraulic pathway.

The relationship between conductivity and pressure is usually defined as a function $k(P)$, commonly known as a vulnerability curve, that incorporates three parameters: a saturated conductivity, a parameter for the pressure at which conductivity is 50% of the saturated value (P_{50}), and a parameter controlling the shape of the curve. To incorporate variation in one or more of these parameters with height along the hydraulic pathway, we write the relationship as

$$k(P,z) = ks(z)f(P,z), \quad (5)$$

with $k_s(z)$ being the saturated conductivity at position z and $f(P, z)$ being a dimensionless vulnerability function that represents the fraction of saturated conductivity that is achieved at a given pressure and position z. The function f incorporates two of the parameters in the relationship $k(P)$ and can allow the dependence of one or more of these parameters on z. Incorporating Equations (4) and (5) into Equation (3) yields

$$Q(z)r(z) + \rho g\alpha(z)f(P,z) = -f(P,z)\frac{dP}{dz}, \quad (6)$$

where r (MPa-s/kg-m) is the resistance per unit length, defined by

$$r(z) \equiv \frac{10^4}{k_s(z)A_s(z)}, \quad (7)$$

and $\alpha(z)$ is the slope of the height function $\tilde{z}(z)$. We can interpret α as the cosine of the average angle of branches of the hydraulic pathway from vertical at point z. When a constant value of α is needed, one could use the average value $\bar{\alpha} = H/L$, where H is the physical height of the tree. Assuming $\alpha = 1$ implies that all branches of the hydraulic pathway are vertical, whereas allowing slightly smaller values for α provides a first-order correction to represent lateral spread of branches.

Equation (6) governs the pressure profile along the stem hydraulic pathway from its base where the boundary condition $P(z = 0) = P_0$ is set.

For the special case in which the parameters of the function f are the same at all points along the hydraulic pathway, we can integrate Equation (6) from the bottom of the stem ($z = 0$) to an arbitrary height:

$$\int_0^z Q(\bar{z})r(\bar{z})d\bar{z} + \rho g\int_0^z \alpha(\bar{z})f(P(\bar{z}))d\bar{z} = \int_{P(z)}^{P(0)} f(\bar{P})\,d\bar{P}. \quad (8)$$

This equation for $P(z)$ can be solved with numerical integration using any vulnerability function for $f(P)$ (Appendix S1), provided that the parameters of this function are uniform along the path length. Equation (8) generalizes the stem MFP model in Sperry et al. (2016; Sperry model) by including continuous variations of A_s, k_s, and of water gravitational potential with z and giving an explicit result for P at all points along the stem hydraulic pathway.

Under the assumptions of the MFP approach (i.e., uniform A_s and k_s, gravity neglected, and "big leaf" canopy confined to the end of the hydraulic path), Q and r are spatially uniform along the stem hydraulic path. The left side of Equation (8) can then be computed to obtain

$$18\times10^{-6}A_lE = \frac{10^{-4}A_sk_s}{z}\int_{P(z)}^{P(0)} f(\bar{P})d\bar{P}. \quad (9)$$

In the Sperry model,

$$18\times10^{-6}A_lE = \frac{10^{-4}A_s}{L}\int_{P_1}^{P_0} k(P)dP, \quad (10)$$

which is a special case of Equation (9) when $z = L$.

3.2 | An analytical solution for the logistic vulnerability function

We now assume that the vulnerability function f includes a parameter $b < 0$ that represents the pressure corresponding to the conductivity $0.5k_s$ (often referred to as P_{50}) and that the vertical variation in the vulnerability function is due to continuous vertical variation in this parameter. Then Equation (6) can be simplified by replacing the dependent variable $P(z)$ with the reciprocal of the fractional loss of conductivity (the percent loss of conductivity [PLC] divided by 100) at each point,

$$Y(z) = \frac{1}{1-f(P,b(z))}, \quad (11)$$

which defines pressure implicitly as $P(Y(z), b(z))$. In terms of this new variable, Equation (6) becomes (see Appendix S1 for detailed derivations)

$$(Y-1)\frac{\partial P}{\partial Y}\frac{dY}{dz} + \left(\frac{\partial P}{\partial b}\frac{db}{dz} + \rho g\alpha(z)\right)(Y-1) + Q(z)r(z)Y = 0. \quad (12)$$

The specific choice of the widely used logistic vulnerability function (Domec & Gartner, 2001; Domec & Pruyn, 2008; Pammenter & Vander Willigen, 1998)

$$f(P,z) = \frac{1}{1+e^{-a[P-b(z)]}} \quad (13)$$

then yields a linear differential equation,

$$\frac{dY}{dz} + a[Q(z)r(z) + B(z)]Y = aB(z), \qquad B(z) \equiv \left(\frac{db}{dz} + \rho g \alpha(z)\right), \quad (14)$$

with boundary conditions,

$$Y(0) = Y_0 \equiv e^{a(P_0 - b_0)} + 1, \qquad P_0 \equiv P(0), \quad b_0 \equiv b(0). \quad (15)$$

This differential equation problem has an analytical solution

$$\begin{aligned} Y &= 1 + e^{-W(z)}\left[Y_0 - 1 - \int_0^z a Q(\hat{z}) r(\hat{z}) e^{W(\hat{z})} d\hat{z}\right], \\ W(z) &= a\int_0^z [Q(\bar{z})r(\bar{z}) + B(\bar{z})]d\bar{z}. \end{aligned} \quad (16)$$

Note that when $P = 0$ and reasonable values of a and b are selected, f is slightly lower than 1, so that the simulated conductivity $k(P = 0)$ is only approximately equal to the parameter k_s (see, for instance, the PLC curves represented in blue in Figure S1). In practice, this approximation is reasonable given that the standard error on measured k_s values typically ranges between 5% and 10% of k_s (Domec, Meinzer, Gartner, & Housset, 2007). Given that vulnerability functions are empirical, the choice of a logistic function does not limit the utility of the analytical result.

In practice, the solution of Equation (14) can be obtained either by using the analytical solution (Equation (16)) with some numerical integration or by using a numerical method to solve the linear differential equation of Equation (14) directly. In the simplified case where Q, r, and α are constant and $b(z)$ is linear, the solution reduces to the explicit formula

$$Y(z) = Y_0 e^{-a(Qr+B)z} + \frac{B}{Qr+B}\left[1 - e^{-a(Qr+B)z}\right]. \quad (17)$$

The quantity B represents the combined effect of gravity and the gradient in b versus height; taking $B = 0$ yields the corresponding result for the standard MFP model. Once Y is determined from Equation (15) or (17), the fractional loss of conductivity is determined as $1/Y$, and the pressure is obtained from Y using Equations (11) and (13):

$$P(z) = b + a^{-1}\ln(Y - 1). \quad (18)$$

Although Equation (17) may be less realistic than Equation (15) because of the additional restrictions, it has the distinct advantage of being an explicit solution formula, rather than a numerical problem. This simplicity arguably makes it preferable for settings in which computational efficiency is imperative.

3.3 | Maximum flow

For a given pressure at the base of the stem, decreasing the pressure at the end of the hydraulic path increases both the cavitation in the column and the flow rate, until a theoretical maximum rate of transpiration produces total cavitation at the end of the hydraulic path (E_{crit}; Tyree & Sperry, 1988; Sperry et al., 2016). Typically, E_{crit} is determined by numerical simulations. However, this definition only makes sense for a big leaf model, in which the transpiration rate of all leaves in the crown is the same. In contrast, because transpiration in our model can vary with the position of the leaf on the hydraulic path, we define an analogous quantity, Q_{crit}, which is the stem-specific maximum total flow rate through the tree for a given water potential at the base of the tree. Our model provides a mathematical definition for Q_{crit}, as the value of $Q_0 = Q(0)$, for which the initial value problem of Equations (14) and (15) yields $Y(L) = 1$, corresponding to $P(L)$ = negative infinity and total cavitation at the end of the pathway. Because the function $Q(z)$ is given in terms of the transpiration $E(z)$ (Equation (2)), the definition of Q_{crit} requires either a big-leaf model or a known transpiration attenuation function $E(z)/E(L)$ in the case where leaves are distributed along the hydraulic path. This value of Q_{crit} can be found for any base pressure P_0 numerically by an iterative scheme that adjusts $E(L)$ until $Y(L) = 1$. If the purpose is to quantify the dependence of the relationship between Q_{crit} and P_0, then it is easier to use assumed values for $E(L)$ to compute $Q(z)$ from Equation (2) and then identify the appropriate Y_0 (and hence P_0 in turn) by integrating Equation (14) backward from $z = L$ to $z = 0$ (Appendix S1). This method allows graphs of Q_{crit} versus P_0 to be obtained with no numerical methods other than a standard numerical differential equation solver. Thus, the value of Q_{crit} indicates the total maximal amount of water that could potentially be transpired per day by a particular tree with given water potential at the base. Because our model incorporates continuous height-related variation in hydraulic parameters, we can analyse the effects of this parameter variation on the maximum flow rate that can be sustained by the stem xylem system.

To find the maximum transpiration rate for the special case in which leaves are all at $z = L$ with constant A_s and k_s, uniform branch angle (constant α), and linear b, we can substitute $Y(L) = 1$ into the analytical solution of Equation (17). This yields an expression for the pressure at the base of the column in terms of Q_{crit},

$$\begin{aligned} P_0 &= b(0) + a^{-1}\ln\left(\frac{rQ_{max}}{rQ_{max} + B}\right) + a^{-1}\ln\left(e^{aL(rQ_{max}+B)} - 1\right), \\ Q_{max} &= 18\times10^{-6} A_T E_{max}, \end{aligned} \quad (19)$$

which defines Q_{crit} implicitly as a function of P_0 and parameters describing the plant hydraulic traits. If the assumptions of constant A_s, k_s, and α and linear b with z are not considered too restrictive, Equation (19) provides a convenient way to calculate Q_{crit} without solving the differential equation (Equations (14) and (15)).

4 | MODEL PARAMETERIZATION

To parameterize our model, we quantified height-related variation in hydraulic traits using data from studies that made measurements at multiple points along the stem height of trees and that reported total tree height. Because hydraulic path lengths are not easily measured, we took measured vertical tree height H as an approximation of path length L and z to be the observation height in fitting models to data. Data were collected from five studies of 11 tree species, for 12 species-by-site combinations (Appendix S3). We examined variation in the Huber value ($h(z) = A_s(z)/A_l(z)$; cm^2/m^2) and k_s with both z and H and variation in two parameters of the logistic vulnerability curve, b (P_{50}) and a, with z. Model parameters were estimated by minimizing the root mean square error (RMSE). RMSE can be interpreted as the standard deviation of the unexplained variance and takes on the same

units as the response variable, and lower values of the RMSE imply better quality of fit (Zar, 1996). *Pseudotsuga menziesii* had the most complete dataset for estimating vertical profiles in hydraulic traits, which were used in the model simulations described in Section 6.

Data on variation in h and k_s with vertical position and tree height were available for only two tree species, *Pseudotsuga menziesii* and *Pinus ponderosa*. For these, h decreased linearly with z, as

$$h(z) = h_0 + zh_s, \tag{20}$$

where h_0 (cm^2/m^2) is the Huber value at the base of the tree and h_s is its rate of change with z (cm^2/m^3; Table 2). Furthermore, h_0 decreased linearly with tree height for both species (Table 2). Vertical variation in k_s was described by a sigmoidal curve that explained a large proportion of the variation in saturated conductivity ($R^2 > 0.75$) and also captured the observed sharp decrease in conductivity near the tree top,

$$ks = \frac{k_0}{1 + (z/Z_{50}L)^{k_{exp}}}, \tag{21}$$

where k_0 (kg/m-s-MPa) is the saturated hydraulic conductivity at the base of the tree ($z = 0$), Z_{50} (dimensionless) is the fraction of L at which k_s is $0.5k_0$, and k_{exp} (dimensionless) is a shape parameter controlling the steepness of the decline in k_s with z. Note that for fitting Equation (21) to data, we assumed $L = H$. Higher values of k_{exp} produce steeper declines in k_s, particularly near the top of the tree, and the optimal parameters for both species are reported in Table 2. Moreover, k_0 increased linearly with tree height for both *P. menziesii* and *P. ponderosa* (Table 2).

To evaluate whether data support our assumptions that the b parameter of the logistic vulnerability curve varies significantly along the hydraulic path (z), we compared the fits of alternative models with data from each species-site combination and compared the quality of the fits of observed PLC values with those predicted by the different models (Appendix S2). A sensitivity analysis showed that the quality of fit was relatively insensitive to the value of a (Figures S2 and S3; Appendix S2), consistent with the common assumption that a vertically uniform value of a is reasonable, which we therefore adopted.

For most trees, PLC curves were measured only at two heights, near the top and at the base, but for one tree, PLC curves were measured at four heights (*P. menziesii*; Domec and Gartner 2001). We therefore tested linear and non-linear variation in b with vertical position for all trees and for the tree with four measurement heights, respectively. Thus, the "linear b model" used a vertically uniform a, and the following equation for b

$$b = b_T + b_s(L - z), \tag{22}$$

where b_T (MPa) is the value of b at the tree top and b_s (MPa/m) is the rate of decline in b with height. For the species with four measurement points, we tested a "non-linear b model," assuming a vertically uniform a and an accelerating decline in b with height,

$$b = b_1 - \frac{b_1 - b_T}{1 + \gamma(L - z)}, \tag{23}$$

where b_T (MPa) is the value of b at the tree top, b_1 is a fitted parameter, and γ (m^{-1}) is a parameter set to 1. Note that for fitting

TABLE 2 Parameter values for hydraulic traits and their variation as a function of height in the tree (z) and, at the base of the tree ($z = 0$), as a function of total tree height ($L \approx H$), for *Pseudotsuga menziesii* and *Pinus ponderosa*

Species	Equation number	*Pseudotsuga menziesii*	*Pinus ponderosa*
L (m)	–	45	40
h_s (cm^2/m^3, uniform models)	20	0	–
h_s (cm^2/m^3, nonuniform models)	20	−0.022	−0.058
$h_0(L)$ (cm^2/m^2, nonuniform models)	20	4.3 − 0.050 L	5.1 − 0.033 L
k_{exp} (dimensionless, uniform models)	21	0	–
k_{exp} (dimensionless, nonuniform models)	21	22	17
Z_{50} (dimensionless, all models)	21	0.93	0.85
$k_0(L)$ ($kg{\cdot}m^{-1}{\cdot}s^{-1}{\cdot}MPa^{-1}$, all models except uniform model from whole stem)	21	1.4 + 0.11 L	1.1 + 0.11 L
a (MPa^{-1}, uniform model from stem base)	–	0.915	–
b (MPa, uniform model from stem base)	–	−3.4	–
a (MPa^{-1}, uniform model from whole stem)	–	1.07	–
b (MPa, uniform model from whole stem)	–	−3.9	–
a (MPa^{-1}, linear b model)	22	1.1	1.6
b_T (MPa, linear b model)	22	−4.2	−5.1[a]
b_s (MPa/m, linear b model)	22	0.022	0.08[a]
a (MPa^{-1}, non-linear b model)	23	1.17	–
b_1 (MPa, non-linear b model)	23	−3.2	–
b_T (MPa, non-linear b model)	23	7.4	–

Note. Parameters and functions are defined in Table 1 and in the main text (see the corresponding equation number). Parameter values were derived from data in Appendix S3 (Domec et al., 2012; Domec & Gartner, 2001; Domec & Gartner, 2002; Domec & Pruyn, 2008; Domec, Pruyn, & Gartner, 2005). Nonuniform and uniform model parameters of *P. menziesii* were used to produce Figures 7 and 8. The uniform model from whole stem has k_s directly calculated to reproduce the K_s of the nonuniform models (e.g., k_s = 3.6 $kg{\cdot}m^{-1}{\cdot}s^{-1}{\cdot}MPa^{-1}$ for 45-m-tall *P. menziesii*). For fitting these models to data, we assumed $L = H$.

[a]Due to the lack of $P_{50}(z)$ data for *P. ponderosa*, an average value across all tall conifers in our database was used instead (Appendix S3).

Equations (22) and (23) to data, we assumed $L = H$. Finally, for all trees, a "uniform a and b model" was also tested, in which both a and b were assumed to be constant with height along the stem.

Most datasets were poorly fit by the uniform a and b model, with an average RMSE of 16% (range: 4.8–35%; Table S1; Figures S1 and S2). The quality of fit for the linear b model (average RMSE of 7.1%; range: 2.5–12%) was consistently better than for the uniform a and b model. Values for b_s varied widely, illustrating that vertical variation in P_{50} differed greatly among tree species, but was significantly greater than zero for all species (Table S1; Figures S1 and S2). Thus, we rejected the hypothesis that the b parameter is uniform with height in these trees. Even though it has the same number of parameters, the model with non-linear, compared with linear, variation in b provided a better fit to the PLC curve of *P. menziesii* from Domec and Gartner (2001), with RMSEs of 4.2% (non-linear) versus 7.9% (linear). In analyses of our vertically explicit model, we therefore contrasted assumptions of linear and non-linear variation in b.

We parameterized our model using published data on hydraulic traits for *P. menziesii* and *P. ponderosa*, for which the most complete data were available (Appendix S3, Table 2). Our goal was not to conduct formal model validation or to fit those particular sets of data per se, but rather to use these data to evaluate the performance of our model and verify that it produced plausible pressure profiles for these empirically measured parameter values. Modelled P profiles were compared with measured xylem P in *P. menziesii* and *P. ponderosa*. Comparisons of data to model predictions demonstrate that our vertically explicit model makes qualitatively correct predictions of these data (Appendix S4, Figure S4).

5 | METHODS OF MODEL ANALYSIS

We used theoretical analyses of our hydraulic model to evaluate the effects of pointwise variation in particular intrinsic and extrinsic hydraulic traits on continuous profiles of P, PLC, and k along the hydraulic path and compared model predictions with and without gravity. Because trees tend to extend further vertically than horizontally, we took vertical height H as an approximation of path length L ($\alpha = 1$) in our simulations. Other values of α can however be used in our model to represent variation in crown architecture. First, we individually varied the slope of the vertical profiles of b (b_s) (Figures 2 and S5a), the shape parameter (k_{exp}) defining variation in the vertical profile of sapwood specific hydraulic conductivity (k_s) (Figures 3 and S5b), and the slope of the vertical profile of the Huber value (h_s) accounting for variation in the sapwood area (Figures 4 and S5c), while keeping the other parameter values constant and equal to values characteristic of *P. menziesii* (Table 3). Although vulnerability segmentation has been observed, branches are often the portion of the tree that is most resistant to cavitation (Johnson et al., 2016), which we also observed in our data analyses (Table 2). For trees of a set height, we therefore modelled declining b with height in the tree (i.e., more negative P_{50} toward the tree top). Trees vary in their patterns of allocation to sapwood. Although higher h characterizes trees with greater water supply capacity per unit leaf area, in the species we considered, h declines with height (Table 2), which leads to relatively lower water supply per unit leaf area in the most distal parts of the tree. We modelled both increasing and decreasing h along the tree height in Figures 4 and S5c. We also examined how P, PLC, and k vary along the hydraulic path for paths of different length (L) given vertical branches ($\alpha = 1$), which corresponds to simulating how these hydraulic profiles change as trees grow to different heights (H; see Figures 5 and S5d). The P_{50} at the topmost branches of the tree has been found to decline with tree height (Ambrose et al., 2009). We examined the effects of this variation on hydraulic function of trees of different heights by conducting simulations with declining b_T with L based on values from *P. menziesii* ($b_T = -5.9$ and -6.6 MPa for 5.6- and 42-m-tall trees, respectively; Domec, Warren, Meinzer, & Lachenbruch, 2009; Figures 5 and S5d).

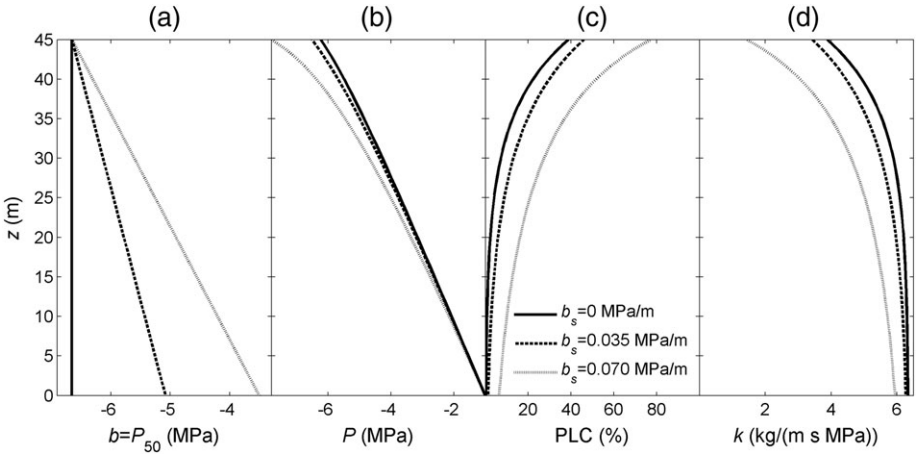

FIGURE 2 Effect of changes in xylem vulnerability to cavitation with position along the hydraulic pathway (z) on xylem pressure and loss of conductivity, including the effect of gravity. (a) The vertical profiles of the pressure at 50% cavitation ($b = P_{50}$) used in simulations, plotted for three values of the slope (b_s) of the $b(z)$ relation, with all other parameters held constant at the values in Table 3. Note that $z = 0$ and 45 m correspond to the base and the top of the tree, respectively. The right panels show vertical profiles driven by the changes in b shown in (a) for (b) xylem pressure (P), (c) percent loss of conductivity (PLC), and (d) hydraulic conductivity ($k = k_s f(P)$). Transpiration rate (E) was set at 7.0 mmol/m^2-s, and E_{crit} was 8.49, 8.00, and 7.22 mmol/m^2-s for scenarios with b_s set at 0, 0.035, and 0.07 MPa/m, respectively

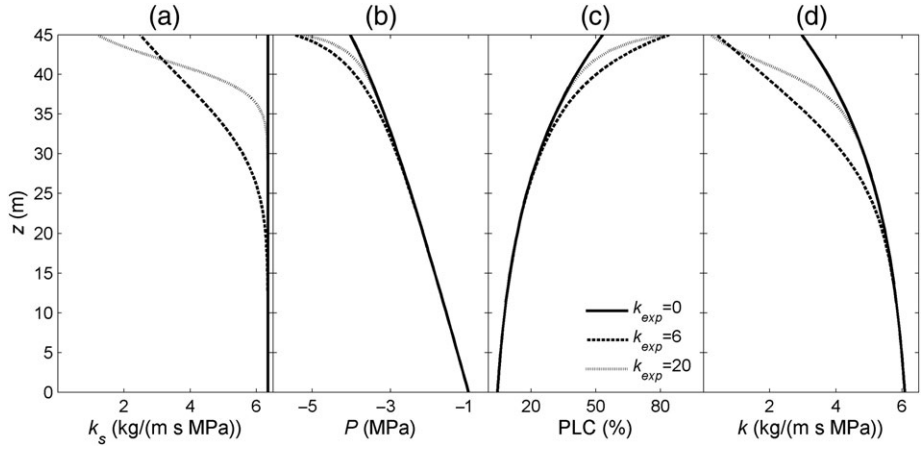

FIGURE 3 Effect of changes in the shape of the saturated hydraulic conductivity (k_s) with position along the hydraulic pathway (z) on xylem pressure and loss of conductivity, including the effect of gravity. (a) The vertical profiles of k_s, plotted for three values of the shape parameter of the $k_s(z)$ function (k_{exp}), with all other parameters held constant at the values in Table 3. Note that z = 0 and 45 m correspond to the base and the top of the tree, respectively. The right panels show vertical profiles driven by changes in k_{exp} for (b) xylem pressure (P), (c) fractional loss of conductivity (PLC), and (d) hydraulic conductivity ($k = k_s f(P)$). Transpiration rate (E) was set at 3.2 mmol/m^2-s, and E_{crit} was 4.23, 3.43, and 3.47 mmol/m^2-s for scenarios with k_{exp} set at 0, 6, and 22, respectively

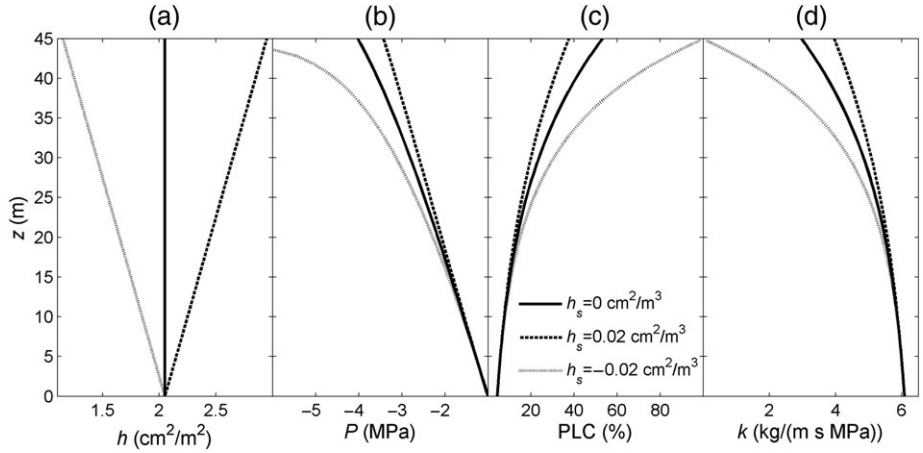

FIGURE 4 Effect of changes in Huber value (sapwood area:leaf area) with position along the hydraulic pathway (z) on xylem pressure and loss of conductivity, including the effect of gravity. (a) The vertical profiles of the Huber value (h) plotted for three values the slope of h versus z (h_s), with all other parameters held constant at the values in Table 3. Note that z = 0 and 45 m correspond to the base and the top of the tree, respectively. The right panels show vertical profiles driven by changes in h_s for (b) xylem pressure (P), (c) fractional loss of conductivity (PLC), and (d) actual hydraulic conductivity ($k = k_s f(P)$). Transpiration rate (E) was set at 3.2 mmol/m^2-s, and E_{crit} was 4.23, 5.12, and 3.20 mmol/m^2-s for scenarios with h_s set at 0, 0.02, and − 0.02, respectively

There is variation in the relationship between k and P along the hydraulic pathway that emerges as a result of vertical variation in b and k_s and due to differences in tree height, H. To understand how the realized vertical progression of hydraulic impairment within a tree differs from the vulnerability curves that can be measured in tissue sampled at a given height, we compared the k–P curves that would be measured empirically from tissue sampled at the tree base or tree top to the emergent, realized relationship as it would vary with z in a tree (Figures 6 and S5e).

Although varying one hydraulic trait at a time isolates the hydraulic effects of that trait, real trees can exhibit simultaneous variation in several traits with z. In Figures 7 and 8, we compared the predictions of our model with vertical variation in b, h, and k_s with the commonly used MFP approach (Equation (10)), which does not allow for such continuous vertical variation. To parameterize our model, we fitted $b(z)$, $k_s(z)$, and $h(z)$ relations (see Section 4 and Appendix S2) using measurements from the literature (Appendix S3). For the MFP model, we used values of b, k_s, and h either measured at the base of *P. menziesii* trees or estimated to reproduce the same stem saturated hydraulic conductance (K_s) as our model (see, for instance, K_s values in Figure 8a). Parameter values can be compared in Figure 7a–c and Table 2. To allow for meaningful comparisons, E was fixed at 2.7 mmol/(m^2-s) and P_0 at 0.5 MPa across models in Figures 7 and 8. Figure 7 focuses on $P(z)$ and $k(z)$ profiles, and Figure 8 addresses tree height-driven variations in K_s, Q_{crit}, maximum PLC, P, and PLC at the top of the tree ($z = L \approx H$). For each scenario, we also calculated E_{crit} (Appendix S1).

TABLE 3 Values and functions of hydraulic traits used in model simulations for Figures 2–5

Baseline parameter values		
a (MPa^{-1})	1.07	Fixed
α (dimensionless)	1	Fixed
b_s (MPa/m)	0	Fixed except in Figures 2 and 5
b_T (MPa)	−3.9	Fixed except in Figures 2 and 5
E ($mmol/m^2$-s)	3.2	Fixed except in Figures 2 and 5
h_0 (L) (cm^2/m^2)	4.3 − 0.050 L	Fixed
h_s (cm^2/m^3)	0	Fixed except in Figure 4
k_0 (L) ($kg{\cdot}m^{-1}{\cdot}s^{-1}{\cdot}MPa^{-1}$)	1.4 + 0.11 L	Fixed
k_{exp} (dimensionless)[a]	0	Fixed except in Figure 3
L (m)	45	Fixed except in Figure 5
P_0 (MPa)	−1	Fixed
Z_{50} (dimensionless)	0.9	Fixed
Varied parameter values		
b_s (MPa/m)	0, 0.035, 0.070	Figure 2
E ($mmol/m^2$-s)	7.0	Figures 2 and 5
k_{exp} (dimensionless)[a]	0, 6, 20	Figure 3
h_s (cm^2/m^3)	−0.02, 0, 0.02	Figure 4
L (m)	15, 30, 45	Figure 5
b_s (MPa/m)	0.070	Figure 5
$b_T(L)$ (MPa)	−5.79 − 0.019 L	Figures 2 and 5

Note. Parameters were fixed at the baseline values, except as noted for a particular figure, in which case they varied as show under "Varied parameter values." Baseline parameter values were derived from data on *Pseudotsuga menziesii*, as detailed in Appendix S3 and Table 2 and described in Section 4. Parameters and functions are defined in Table 1.

[a]When k_{exp} = 0, the value of k_0 is multiplied by 2 to obtain the same k_s (z = 0) as with k_{exp} > 0 (Equation (19)).

6 | RESULTS OF MODEL ANALYSIS

6.1 | Effects of vertical variation in hydraulic traits and gravity on hydraulic function

In general, P becomes more negative, PLC increases, and k decreases with increasing height in a tree (Figures 2–5 and S5). However, the specific shapes of the curves defining these changes in P, PLC, and k depend on vertical gradients in intrinsic and extrinsic trait values and the effect of gravity. Higher values of b_s generate greater differences in b from the bottom to the top of the tree, indicating xylem cavitation at progressively less negative P (Figure 2a). The decline in P with height in the tree accelerates as the difference in b from the bottom to the top of the tree increases (Figure 2b). Hydraulic conductivity hence becomes impaired at progressively lower heights compared with the case of a vertically uniform b and as b_s increases and E becomes closer to E_{crit} (Figure 2c,d).

Relative to the case of vertically uniform saturated conductivity fixed at the tree-base value, k_0 (solid line, k_{exp} = 0), increasing k_{exp} causes k_s to remain closer to k_0 further up the tree, until k_s declines rapidly (Figure 3a). Thus, the larger the k_{exp}, the higher in the tree and the more rapid the change in the deviation of PLC and P is from the case of no vertical variation in k_s (Figure 3b,c). This effect is due to the lower k_s in the middle section of the tree caused by the lower, nonzero value of k_{exp}, which causes reductions in k also to occur at lower heights along the tree (Figure 3d). With k_{exp} = 20, there is efficient water transport even into the middle section of the tree, and conductivity decreases sharply only toward the very top (Figure 3d), where water transport is hampered (Figure 3a) and declining pressure (Figure 3b) and cavitation (Figure 3c) become apparent.

With negative values of h_s, there is progressively less sapwood area along the hydraulic pathway to supply the leaf area. Hence, P declines faster with height in the tree with negative h_s compared with the case with no vertical variation in h_s or positive h_s (Figure 4b),

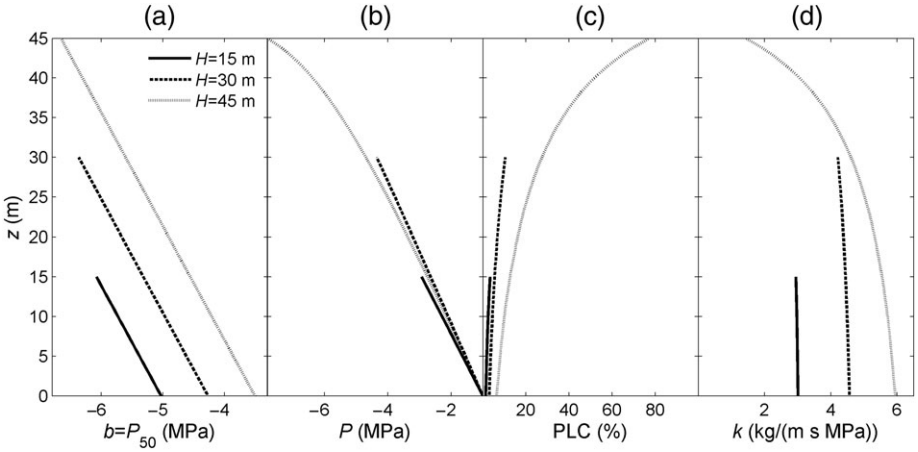

FIGURE 5 Combined effects of changes in tree height (H) and xylem vulnerability (b) with position along the hydraulic pathway (z) on xylem pressure and conductivity, including the effect of gravity. (a) The vertical profiles of the pressure at 50% cavitation ($b = P_{50}$), plotted for three values of tree height H, assuming the declining b_T for trees of increasing heights and a fixed slope of the $b(z)$ relation, with all other parameters held constant at the values in Table 3. Note that z = 0 and $z = H$ correspond to the base and the top of the tree, respectively, because we assumed α = 1 and $L = H$. The right panels show vertical profiles driven by changes in H as described in (a) for (b) xylem pressure (P), (c) percent loss of conductivity (PLC), and (d) hydraulic conductivity ($k = k_s f(P)$). Transpiration rate (E) was set at 7.0 $mmol/m^2$-s, and E_{crit} was 19.0, 11.3, and 7.2 $mmol/m^2$-s for scenarios with H set at 15, 30, and 45 m, respectively

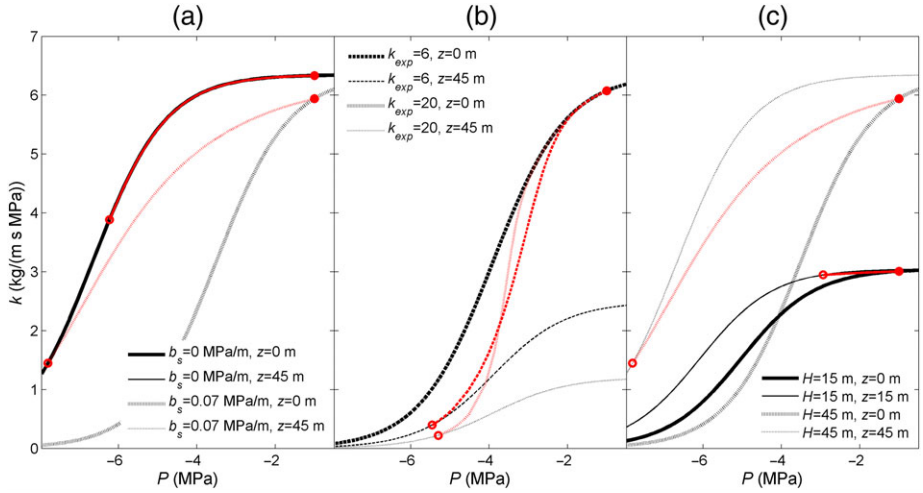

FIGURE 6 Changes in stem hydraulic conductivity ($k = k_s f(P)$) as a function of xylem pressure (P) as they are realized along the tree height, for contrasting scenarios corresponding to Figures 2, 3, and 5: (a) different values of b_s, the slope of the vertical profile of the pressure at 50% cavitation ($b = P_{50}$) for fixed H and k_s, as in Figure 2; (b) different curvatures for the vertical profile in saturated conductivity (k_{exp}), as in Figure 3; and (c) different tree heights (H) and pressures at 50% cavitation at the top of the stem (b_T), as in Figure 5. Because we assumed $\alpha = 1$, $L = H$. Black curves represent conductivity–pressure relations at a given height as would be measured in tissue samples extracted from height z. The red curves represent the realized k–P relationship predicted by our model as it varies from the base to the top of the tree. There are only two red curves in each panel because each is equivalent to a phase-space representation across all z, and two sets of parameter values are represented. For the red curves, closed (●) and open (○) circles indicate the values at the tree base and tree top, respectively. For parameter values, dashing style for the red curves corresponds to those for the black curve). In (a), the thick and thin solid black curves and the thin dotted black curve overlap, because they share the same value of b; in (c), the thick dashed and dotted black curves overlap because at the tree base, k_s is the same. If there is no vertical variation in hydraulic traits, then the red and black curves overlap (e.g., in (a)) [Colour figure can be viewed at wileyonlinelibrary.com]

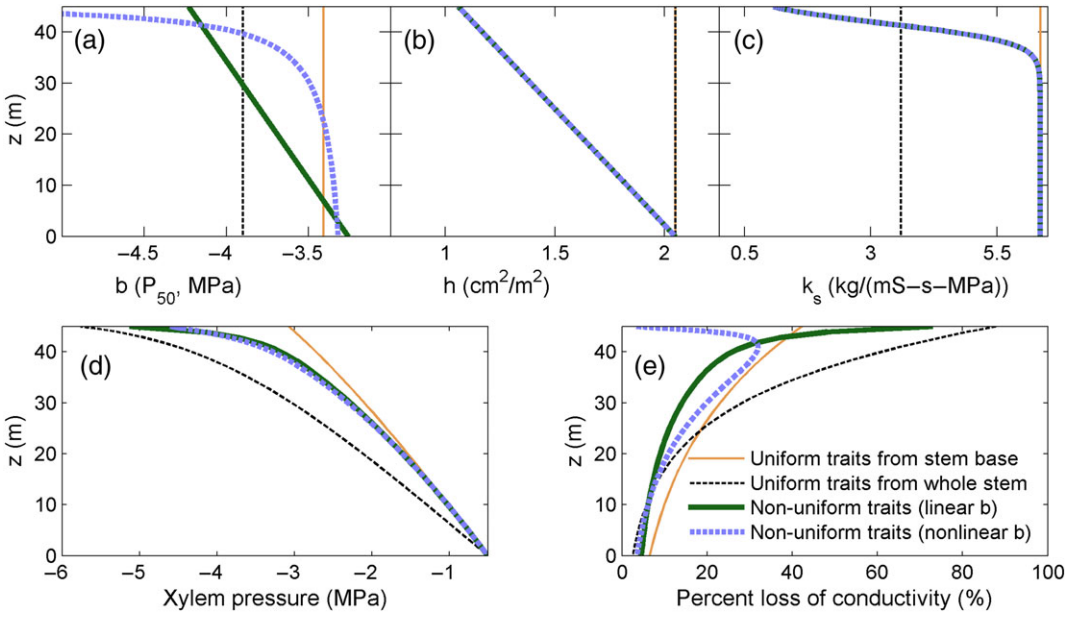

FIGURE 7 Comparison of predictions from the vertically explicit model presented here to the matric flux potential (MFP) model for variation in hydraulic function with position along the hydraulic path. (a–c) The modelled relationships for variation in the pressure at which 50% of the stem conductivity is lost ($b = P_{50}$), the Huber ratio (h), and saturated hydraulic conductivity (k_s), respectively, with position along the hydraulic path (z) (see parameter values in Table 2). The different curves represent scenarios with varying complexity of vertical variation in hydraulic traits, with the MFP model parameterized with either uniform trait values corresponding to those measured at the base of the tree (solid gold) or uniform trait values estimated to match the K_s of vertically nonuniform models (dotted black; here, k_s = 3.6 kg·m^{-1}·s^{-1}·MPa^{-1}), compared with our vertically explicit model with continuous variation in traits parameterized with either linear $b(z)$ (solid thick green) or non-linear $b(z)$ (dashed blue). The effects of these four contrasting scenarios on the vertical profiles in hydraulic function are shown for xylem pressure (D) and percent loss of conductivity, PLC (E). Note that H = 45 m, P_0 = 0.5 MPa, and E = 2.7 mmol/(m^2-s) across scenarios. Transpiration rate (E) was set at 2.7 mmol/m^2-s, and E_{crit} was 4.33, 2.82, 2.95, and 3.25 mmol/m^2-s, respectively, for scenarios with uniform trait values corresponding to those measured at the base of the tree (solid gold) or estimated to match the K_s of vertically nonuniform models (dotted black) and with continuous variation in traits parameterized with either linear $b(z)$ (solid thick green) or non-linear $b(z)$ (dashed blue). [Colour figure can be viewed at wileyonlinelibrary.com]

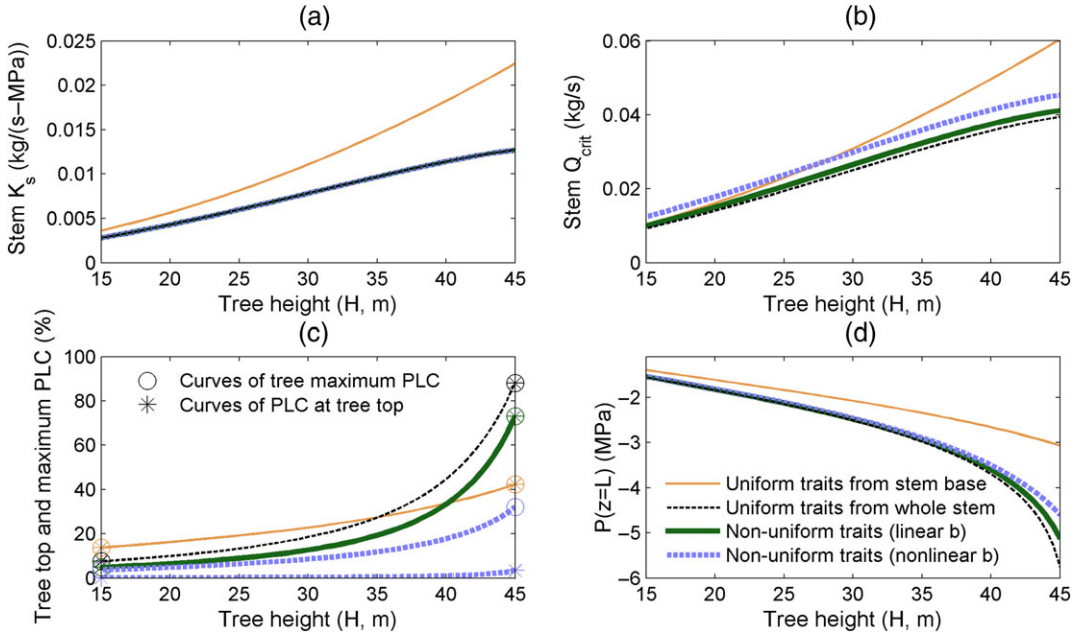

FIGURE 8 Comparison of predictions from the vertically explicit model presented here to the matric flux potential (MFP) model for variation in hydraulic function with tree height (H). Because we assumed α = 1, $L = H$. The different curves represent scenarios with varying complexity of vertical variation in hydraulic traits, with the MFP model parameterized with either uniform trait values corresponding to those measured at the base of the tree (solid gold) or uniform trait values estimated to match the K_s of vertically nonuniform models (dotted grey) compared with our vertically explicit model with continuous variation in traits parameterized with either linear $b(z)$ (solid thick green) or non-linear $b(z)$ (dashed blue). The effects of these four contrasting scenarios on the vertical profiles in hydraulic function are shown for saturated stem conductance, (a) K_s, stem-specific theoretical maximum flow rate before hydraulic failure, (b) Q_{crit}, the maximum percent loss of conductivity (PLC) and PLC at the top of the tree (c) ($z = L$), and xylem pressure at the top of the tree, (d) $P(z = L)$. Note that traits in Figure 7 are varied as illustrated in Figure 7a–c, and parameter values determining these properties correspond to those for *P. menziesii* (Table 2), with P_0 = 0.5 MPa, and E = 2.7 mmol/(m^2-s). Note that in Figure 8A, with the exception of the gold curve, the scenarios modelled in all curves (which cannot be distinguished because they overlap) were designed to have the same variation in K_s with H, in order to compare the impact of uniform versus nonuniform hydraulic traits given the same K_s. Because the gold curve uses trait values from the stem base, by definition, it cannot have the same K_s as the other curves [Colour figure can be viewed at wileyonlinelibrary.com]

causing cavitation at lower heights (Figure 4c), with corresponding declines in k (Figure 4d). Although we modelled parameter values that were symmetrical around h_s = 0, the effects on hydraulic function are not symmetrical because with declining h, there is progressively less sapwood, causing frictional pressure losses to continue to worsen due to resistance caused by the lengthening hydraulic path. Positive h_s compensates for these losses and allows maintenance of higher P and k (Figure 4b,d), with associated reductions in PLC and increases in E_{crit} (Figure 4c). Vertical variation in A_s (here accomplished through h_s) and k_s has similar impacts on the pressure profile (Figures 3 and 4), but generates compounded effects when more realistic parameterizations are selected as described below.

The effects of increasing tree height H and decreasing b_T on P and PLC become most noticeable in the tallest simulated tree (45 m; Figure 5). In this scenario, the fixed b_s increases b_0 by 0.07 MPa for each extra meter of tree height, whereas the $b_T(L \approx H)$ relation tends to decrease b_0 by only 0.019 MPa/m. Consequently, b_0 must increase with H (Table 3, Figure 5a), consistent with observations of positive scaling of xylem and stem diameter (Olson & Rosell, 2013). At a given height within the tree, taller trees are both more sensitive to cavitation (Figure 5a) and more conductive (Figure 5d) than shorter trees, in agreement with observations (Figure S2, Appendix S3). Because of the combined effects of higher conductivity and greater sensitivity to cavitation at the tree base, taller trees exhibit similar pressure drops with z as smaller trees, for a given transpiration rate (Figure 5b). However, the tallest tree's low E_{crit} was closest to E, causing PLC to increase the fastest, especially towards the top of the tree (Figure 5c). There were corresponding decreases in k (Figure 5d) due to the accumulation of cavitation resulting from the greater vulnerability of the xylem for most of the path length of tall trees (Figure 5a).

Comparing results from simulations that are otherwise identical, but either include (Figures 2–5) or exclude (Figure S5) the effect of gravity allows examination of how vertical variation in hydraulic traits interacts with gravity to affect hydraulic function. In general, relative to the case without gravity, gravity causes reductions in P to accelerate faster with z, which causes PLC to increase and k to decrease at ever-faster rates with height in the tree. These effects are particularly acute when vertical variation in hydraulic traits is such that the sapwood at the base of the tree has greater conducting capacity (Figures 4 and S5c) or greater vulnerability (Figures 2 and S5a) relative to the top of the tree, which is often the case for tall trees (Figures 5 and S5d). This is because any form of vertical variation in traits that causes progressively less water to be supplied to the higher portions of the tree, such as via reduced sapwood area with height (Figures 4 and S5c) or via increased cavitation at the tree base (Figures 2 and S5a), has magnifying effects on P that are compounded by gravity and that reduce E_{crit}. Because E is fixed, these trees are operating closer to the limits of their hydraulic system, which manifests in our results as

accelerating hydraulic impairment with height in the tree. In other words, gravity has a stronger effect on water flow as E gets closer to E_{crit}, and the shapes of the curves describing how vertical variation in hydraulic traits affects hydraulic function are defined by the effect that the trait has on E_{crit} and how close E is to that E_{crit} value.

Our model enables us to predict the actual vulnerability curve realized along the entire hydraulic path of the stem and compare them with measured *PLC* curves from particular heights in a tree (Figure 6) to visualize the vertical progression of hydraulic impairment in the stem. Each realized $k(P)$ curve in Figure 6 connects the k and P pairs on the *PLC* curve measured at the base of the tree to the corresponding point on the *PLC* curve at the tree top. This comparison shows that the realized whole-stem vulnerability curve (red curves) differs from the measured *PLC* curves (black curves) and is an emergent property that depends on the current transpiration rate and the compounding effects of continuously varying intrinsic and extrinsic hydraulic properties on the pointwise feedback between k and P. Differences between these curves within and across panels are caused by changes in intrinsic traits and tree height. Because P declines with height in the tree at a faster rate when b changes vertically compared with the case of invariant b (Figure 2), the model predicts larger changes in the realized vulnerability curve from the tree base to the top in the former case ($b_s > 0$; dotted red curve in Figure 6a). Steeper $k_s(z)$ allows a relatively higher conductivity to be maintained despite declining P until there is a precipitous drop in conductivity at the top of the tree, at which point a tree with shallower $k_s(z)$ maintains higher conductivity (Figure 3). This explains the crossing between the realized $k(P)$ relations shown in Figure 6b. The contrasting vertical parameter profiles of tall versus short trees (Figure 5) result in larger changes in pressure and conductivity from the tree base to the canopy in taller trees (dot-dashed vs. solid red curve in Figure 6c). The effect of gravity is to produce wider ranges of k and P across the tree, particularly causing more negative values towards the top of the tree (Figures 6 and S5e).

6.2 | Comparing model predictions assuming vertical variation in multiple hydraulic traits

We compared predictions for stem vertical profiles in P (Figure 7d) and *PLC* (Figure 7e) from our model (thick green and blue curves) with an MFP model (thin gold and black curves) incorporating gravity and with several scenarios of vertical variation in multiple hydraulic traits for a 45-m-tall tree (Figure 7a–c). Using these models and parameterizations, we also compared predictions of variation in Q_{crit} (Figure 8b), the maximum *PLC* and *PLC* at the top of the tree (Figure 8c), and P at the top of the stem (Figure 8d) for trees 15–45 m tall. All parameter values were chosen so that stem K_s was the same across models and parameterizations, with the exception of the MFP model parameterized using uniform traits from the stem base (Figure 8a).

All models and parameterizations predicted monotonically declining P with height z in the stem (Figure 7d). However, the MFP models parameterized with uniform traits from the stem base and a whole-stem average overpredicted and underpredicted, respectively, the vertical profile in P, compared with our model parameterized with nonuniform traits. Moreover, in our model, assuming linear or non-linear vertical variation in b produced similar P profiles (Figure 7d). Predictions were more variable across models for the vertical profile of *PLC* (Figure 7e). The MFP model parameterized with whole-stem values overpredicted *PLC* at taller heights in the stem and underpredicted *PLC* lower down in the stem, relative to the MFP model with stem-base values and our model. For the MFP model with stem-base values, *PLC* gradually increased but remained low even towards the top of the stem, whereas assuming linear variation in b in our model caused *PLC* to rapidly increase at the very top of the stem while remaining low at lower heights. Our model parameterized using non-linear variation in b produces a *PLC* curve resembling that of the MFP model parameterized with uniform, stem-base traits, until the very top of the stem, at which point *PLC* declines rapidly even though the P profile does not (Figure 7d). The rapid drop in *PLC* occurs because, with the non-linear b parameterization, xylem vulnerability rapidly declines (Figure 7a) at the top of the stem, but the P profile is determined more by water flow upstream (at lower heights) in the stem.

For all models and parameterizations, Q_{crit} increased monotonically across trees of different heights H (Figure 8b). With uniform stem-base traits, the MFP model predicted Q_{crit} to increase more rapidly towards the top of the stem than the other models and parameterizations did. In contrast, of the other three models and parameterizations, our model with non-linear vertical variation in b predicted the highest Q_{crit}, which happens because Q_{crit} is largely determined by hydraulic function toward the top of the stem, where the non-linear b parameterization has low xylem vulnerability (Figure 7a) and low *PLC* (Figure 7e).

Curves describing the variation among trees of different heights in maximum *PLC* observed in the stem and the *PLC* at the stem top coincided for all models and parameterizations except our model parameterized with non-linear variation in b (dashed blue curve in Figure 8c). For this parameterization, the *PLC* at the stem top remained low across all tree heights, and the maximum *PLC* occurred at a lower height in the stem. Stem-top and maximum *PLC* increased more rapidly for the tallest trees in the MFP model with uniform whole-stem traits and in our model with linear variation in b. In contrast, the MFP model with stem-base traits (red curve in Figure 8) did not exhibit such steep increases and predicted higher maximum and stem-top *PLC* for shorter trees, but lower *PLC* for taller trees. This variation corresponds to the predictions for P at the top of the stem (Figure 8d), in which the MFP model with stem-base traits predicted higher stem-top P for all tree heights and did not exhibit the rapid decline in stem-top P for the tallest trees predicted by the other three models and parameterizations, which exhibited similar behaviour.

7 | DISCUSSION

The ability to accurately model water transport in trees, especially tall trees, is critical for predicting how forests respond to environmental stress. We present the first hydraulic model of water transport in stems that incorporates continuous vertical profiles of both intrinsic and extrinsic hydraulic traits in tree stems. Our reference point for model development was Sperry's MFP model (Sperry et al., 1998; Sperry et al., 2016), which our model generalizes by including the

effects of gravity and by allowing transpiration, leaf area, sapwood-saturated conductivity, the vulnerability curve parameter P_{50}, and the Huber ratio to vary along the hydraulic path. These generalizations are important because under nonstressful growing conditions, our model makes predictions that differ from the Sperry model about how hydraulic function changes with height in a tree and across trees of different heights.

Many intrinsic and extrinsic stem hydraulic traits affect vertical profiles of *k*, *P*, and *PLC* in tree stems and thereby mediate hydraulic function of trees. Our literature review showed that, across a diverse array of tree species, these hydraulic traits vary along the hydraulic path of stems. Our model analyses show that their compounded effect produces different vertical profiles of hydraulic function than in the case with vertically uniform traits. Importantly, accounting for the non-linear compounding effect generated by vertical variation in intrinsic and extrinsic stem hydraulic traits is a significant advance. This vertical variation in hydraulic traits acts to counter the impairment of water transport that accelerates with length along the hydraulic path (Zimmerman, 1983) and due to the effects of gravity (Tyree & Ewers, 1991), thereby helping to maintain whole-tree hydraulic integrity while allowing trees to operate near their hydraulic capacity (Choat et al., 2012; Tyree & Sperry, 1988). Although building more resistant xylem counters the increasingly negative effects of gravity and path length resistance on pressure, it also restricts water flow, which would ultimately limit tree height (Koch et al., 2004; Ryan & Yoder, 1997). Thus, other traits must co-vary with *b* to ensure a hydraulically safe xylem while also allowing sufficient turgor pressure for cell expansion and growth at the top of the tree (Woodruff, Bond, & Meinzer, 2004).

Our model analyses demonstrate that growing more sapwood to increase *h* as trees age (e.g., McDowell et al., 2002), xylem tapering with larger k_s at the tree base (Olson & Rosell, 2013; Savage et al., 2010; West et al., 1999), and reducing xylem vulnerability only at the most distal portions of the stem while maintaining transport capacity at the base (e.g., Johnson et al., 2016) allow tall trees to compensate for these effects. We also show that height-driven, continuous declines in *b* and k_s, as indicated by the well-known pattern of declining conduit diameter from the base to the apex of the stem (Petit, Pfautsch, Anfodillo, & Adams, 2010; West et al., 1999), cause vertical variation in pressure that increases cavitation mainly at the top of the tree. As a result, the largest hydraulic resistance in stems occur at the apices, so that realized conductivity does not decline linearly with plant height (Petit et al., 2010). Non-linear declines in *b* with height were found to be particularly protective and allow maximal *PLC* to remain low while ensuring water flow, even for the tallest tree in our simulations (45 m). For it, the maximal *PLC* did not occur at the tree top, but at a slightly lower height, consistent with drought-induced shoot die-back, which limits damage to the portions of the hydraulic pathway that can be sacrificed with minimal cost (Davis et al., 2002), consistent with the multiple leaders seen in tall redwoods (Koch et al., 2004). These ecologically realistic results highlight the ability of our model to predict the consequences of ontogenetic and height-related changes in hydraulic traits and the changing environmental stresses that accompany tree growth. Moreover, our model demonstrates that the ability to achieve similar hydraulic performance through different combinations of height-related variation in hydraulic trait values is evidence of phenotypic integration (Pigliucci & Preston, 2004), which makes it challenging to identify well-constrained rule sets describing variation in hydraulic traits as a function of the environment, tree species' ecological strategy and growth form, and tree height (e.g., Bartlett, Klein, Jansen, Choat, & Sack, 2016).

7.1 | Theoretical advances

Because water potential controls gas exchange rates (Lawlor & Tezara, 2009; Sack & Holbrook, 2006) and hydraulic damage during droughts (Mencuccini et al., 2015), its accurate prediction along the hydraulic pathway is key to understanding and predicting whole-plant responses to environmental stress. Although analytical solutions of water pressure profiles accounting for continuously changing properties were recently developed for roots (Meunier, Couvreur, Draye, Vanderborght, & Javaux, 2017a; Meunier, Couvreur, Draye, Vanderborght, & Javaux, 2017b; Meunier, Draye, et al., 2017), we are the first to develop them for stems for both intrinsic and extrinsic hydraulic traits. Several assumptions required in existing stem hydraulic models are relaxed in our framework. As currently implemented, MFP and continuous models assume sapwood area-preserving branching (West et al., 1999), uniform sapwood saturated conductivity, uniform vulnerability curve parameters (Bohrer et al., 2005; Mirfenderesgi et al., 2016; Sperry et al., 1998), and uniform Huber ratio (Sperry et al., 1998) within a segment of the hydraulic pathway. By recasting Darcy's law (Equation (1)) in terms of cavitation rather than pressure, we obtained an ordinary differential equation that allows the derivation of an analytical solution to the continuous Darcy's law equation. Our model ignores water storage, which produces diurnal variation in pressure, but does not create significant differences in daily averages during long periods of relatively stable environmental conditions, because stem water storage relaxation times are shorter than a day (Phillips et al., 1997). Our model also does not explicitly describe complex crown architecture, which is challenging given the vast diversity of branching patterns observed among tree species (Halle, Oldeman, & Tomlinson, 1978). Explicitly accounting for crown architecture also requires complex segmentation in models (e.g., Bohrer et al., 2005), which increases the computation time required to solve the model. However, our model implicitly accounts for tree architecture, thereby continuing to accurately capture *k*–*P* feedbacks arising along the entire hydraulic path while still allowing for branching and for leaves to be distributed at any point along the hydraulic path.

We derived a differential equation to determine the pressure at any point on the hydraulic pathway, given the hydrostatic pressure at the base of the stem (P_0) and the transpiration rate (*E*). Solving discrete models, MFP models, and continuous models with segments requires complex numerical solutions. In contrast, under the most general case, our model can be solved using a far simpler numerical solution (Equation (14)) and, for a more restricted set of assumptions, can be solved analytically (Equation (18)). Our model thus makes it possible to easily determine the impact of vertical variation in traits on hydraulic function, because computationally efficient and accurate predictions of stem water flow, pressure, conductivity, and

conductance can be made at any point along the hydraulic path. These novel modelling capabilities are fundamental to linking trait variation to community- and ecosystem-level processes as earth systems models transition from parameterizations based on plant functional types to trait-based parameterizations (van Bodegom et al., 2014; Wang et al., 2017). Moreover, our hydraulic model is computationally simple, making it feasible to incorporate into ecological models, such as dynamic global vegetation models.

Previous models defined the theoretical maximum transpiration rate (E_{crit}; the transpiration rate for which cavitation approaches 100%; Sperry et al., 2016; Tyree & Sperry, 1988), which can be calculated analytically, for a discrete model limited to well-watered conditions (Manzoni et al., 2013), or numerically, based on a minimum physiologically relevant conductance value (Sperry, Hacke, Oren, & Comstock, 2002). Our model provides an analytical solution for the stem E_{crit} while accounting for gravity, accommodating continuously varying hydraulic traits, and when leaves are distributed along the hydraulic pathway, which is not possible in MFP or continuous models. The E_{crit} predicted by our model, however, accounts for hydraulic failure only in the stem, neglecting hydraulic bottlenecks at the soil-root interface and in leaves. It therefore constitutes an upper bound to the maximum transpiration rate as constrained by hydraulic processes operating across the entire stem. For this reason, we also derived Q_{crit}, which describes the theoretical maximum water flow rate through the stem that a given tree can sustain. Because Q_{crit} is a property that does not vary if the amount of leaves increases proportionally, whereas E_{crit} does, it provides a good description of stem hydraulic limitations on water flow.

7.2 | Conclusion: The adaptive significance of vertical variation in hydraulic traits

A continuous solution for xylem pressure allows for more accurate modelling of hydraulic function at any point on the tree (Bohrer et al., 2005). Our vertically explicit, analytical model of water transport not only provides this but also formalizes the critical links between vertical variation of intrinsic and extrinsic hydraulic traits, the development of cavitation, and water transport capacity in tree stems. Because vertical trait variation counters the negative effects of gravity and path length on pressure, it contributes to allowing trees to grow taller into environments that provide ever-better insolation, but that are hydraulically more stressful due to greater heat load and evaporative demand (Ryan & Yoder, 1997). If a tree has an optimal balance between allocation to root, stem, and leaf function for its environment, then it should often be operating near its hydraulic capacity (Choat et al., 2012; Tyree & Sperry, 1988). The adaptive significance of vertical variation in stem hydraulic traits is to allow trees to operate near their hydraulic limits, that is, when E is close to E_{crit}, and to push the boundaries of those hydraulic limits. Tall trees are a quintessential example of plants pushing hydraulic limits (Koch et al., 2004; Ryan & Yoder, 1997), and so it is not surprising that most empirical studies of vertical variation in hydraulic traits have been conducted on species reaching some of the tallest heights on Earth. Although less explored, vertical variation in hydraulic traits is likely to be important even in species with shorter maximum height. Our model analyses therefore provide theoretical motivation for more empirical studies to quantify vertical variation in and coordination among hydraulic traits in a wider array of tree species with varying ecological strategies.

ACKNOWLEDGMENTS

We thank Gil Bohrer and two other reviewers for constructive comments on an earlier version of this manuscript. This work was developed during working group meetings at the National Institute for Mathematical and Biological Synthesis (NIMBIOS; DEB Model for Trees) sponsored by the National Science Foundation through NSF Award DBI-1300426, with additional support from The University of Tennessee, Knoxville, and at the University of Nebraska-Lincoln (UNL), sponsored by the UNL College of Arts and Sciences International Research Collaborations Award. S.M. was partly supported by the Swedish Research Council Formas (2016-00998). G.L. was partly supported as a Sabbatical Fellow at NIMBIOS. D.W. was partly supported by the Canadian Natural Sciences and Engineering Research Council and an Ontario Early Career Award. V.C. was partly supported by the Interuniversity Attraction Poles Programme—Belgian Science Policy (Grant IAP7/29), by the "Communauté française de Belgique-Actions de Recherches Concertées" (Grant ARC16/21-075), by the "Belgian American Educational Foundation" (BAEF) as UCLouvain Fellow, by "Wallonie-Bruxelles International" (WBI) with a WBI. WORLD excellence grant, and by the "Fonds Spéciaux de Recherche" (FSR) of the Université Catholique de Louvain. Part of this work was conducted while S.E.R. and G.L. were on Faculty Development Leave from UNL. The authors declare no conflicts of interest.

ORCID

Valentin Couvreur http://orcid.org/0000-0002-1087-3978
Danielle A. Way http://orcid.org/0000-0003-4801-5319
Sabrina E. Russo http://orcid.org/0000-0002-6788-2410

REFERENCES

Ambrose, A. R., Sillett, S. C., & Dawson, T. E. (2009). Effects of tree height on branch hydraulics, leaf structure and gas exchange in California redwoods. *Plant, Cell & Environment*, *32*, 743–757.

Aumann, C. A., & Ford, E. D. (2002). Modeling tree water flow as an unsaturated flow through a porous medium. *Journal of Theoretical Biology*, *219*, 415–429.

Bartlett, M. K., Klein, T., Jansen, S., Choat, B., & Sack, L. (2016). The correlations and sequence of plant stomatal, hydraulic, and wilting responses to drought. *Proceedings of the National Academy of Sciences*, *113*, 13098–13103.

Bennett, A. C., McDowell, N. G., Allen, C. D., & Anderson-Teixeira, K. J. (2015). Larger trees suffer most during drought in forests worldwide. *Nature Plants*, *1*, 15139.

van Bodegom, P. M., Douma, J. C., & Verheijen, L. M. (2014). A fully traits-based approach to modeling global vegetation distribution. *Proceedings of the National Academy of Sciences*, *111*, 13733–13738.

Bohrer, G., Mourad, H., Laursen, T. A., Drewry, D., Avissar, R., Poggi, D., … Katul, G. G. (2005). Finite element tree crown hydrodynamics model (FETCH) using porous media flow within branching elements: A new representation of tree hydrodynamics. *Water Resources Research*, *41*. W11404

Brienen, R. J. W., Gloor, E., Clerici, S., Newton, R., Arppe, L., Boom, A., … Timonen, M. (2017). Tree height strongly affects estimates of water-

use efficiency responses to climate and CO_2 using isotopes. *Nature Communications*, *8*, 288.

Burgess, S. S. O., Pittermann, J., & Dawson, T. E. (2006). Hydraulic efficiency and safety of branch xylem increases with height in *Sequoia sempervirens* (D. Don) crowns. *Plant, Cell & Environment*, *29*, 229–239.

Čermák, J., Kučera, J., Bauerle, W. L., Phillips, N., & Hinckley, T. M. (2007). Tree water storage and its diurnal dynamics related to sap flow and changes in stem volume in old-growth Douglas-fir trees. *Tree Physiology*, *27*, 181–198.

Choat, B., Jansen, S., Brodribb, T. J., Cochard, H., Delzon, S., Bhaskar, R., … Zanne, A. E. (2012). Global convergence in the vulnerability of forests to drought. *Nature*, *491*, 752.

Christoffersen, B. O., Gloor, M., Fauset, S., Fyllas, N. M., Galbraith, D. R., Baker, T. R., … Meir, P. (2016). Linking hydraulic traits to tropical forest function in a size-structured and trait-driven model (TFS v.1-Hydro). *Geoscientific Model Development*, *9*, 4227–4255.

Chuang, Y. L., Oren, R., Bertozzi, A. L., Phillips, N., & Katul, G. G. (2006). The porous media model for the hydraulic system of a conifer tree: Linking sap flux data to transpiration rate. *Ecological Modelling*, *191*, 447–468.

Comstock, J. P., & Sperry, J. S. (2000). Tansley Review No. 119: Theoretical considerations of optimal conduit length for water transport in vascular plants. *New Phytologist*, *148*, 195–218.

Couvreur, V., Vanderborght, J., Beff, L., & Javaux, M. (2014). Horizontal soil water potential heterogeneity: Simplifying approaches for crop water dynamics models. *Hydrology and Earth System Sciences*, *18*, 1723–1743.

Cruiziat, P., Cochard, H., & Améglio, T. (2002). Hydraulic architecture of trees: Main concepts and results. *Annals of Forest Science*, *59*, 723–752.

Darcy, H. (1856). *Les fontaines publiques de la ville de Dijon*. Paris: Dalmont.

Davis, S. D., Ewers, F. W., Sperry, J. S., Portwood, K. A., Crocker, M. C., & Adams, G. C. (2002). Shoot dieback during prolonged drought in *Ceanothus* (Rhamnaceae) chaparral of California: A possible case of hydraulic failure. *American Journal of Botany*, *89*, 820–828.

Delzon, S., Sartore, M., Burlett, R., Dewar, R., & Loustau, D. (2004). Hydraulic responses to height growth in maritime pine trees. *Plant, Cell & Environment*, *27*, 1077–1087.

van den Honert, T. H. (1948). Water transport in plants as a catenary process. *Discussions of the Faraday Society*, *3*, 146–153.

Domec, J. C., & Gartner, B. L. (2001). Cavitation and water storage capacity in bole xylem segments of mature and young Douglas-fir trees. *Trees-Structure and Function*, *15*, 204–214.

Domec, J. C., & Gartner, B. L. (2002). Age- and position-related changes in hydraulic versus mechanical dysfunction of xylem: inferring the design criteria for Douglas-fir wood structure. *Tree Physiology*, *22*, 91–104.

Domec, J. C., Lachenbruch, B., Pruyn, M. L., & Spicer, R. (2012). Effects of age-related increases in sapwood area, leaf area, and xylem conductivity on height-related hydraulic costs in two contrasting coniferous species. *Annals of Forest Science*, *69*, 17–27.

Domec, J.-C., Meinzer, F. C., Lachenbruch, B., & Housset, J. (2007). Dynamic variation in sapwood specific conductivity in six woody species. *Tree Physiology*, *27*, 1389–1400.

Domec, J. C., & Pruyn, M. L. (2008). Bole girdling affects metabolic properties and root, trunk and branch hydraulics of young ponderosa pine trees. *Tree Physiology*, *28*, 1493–1504.

Domec, J. C., Pruyn, M. L., & Gartner, B. L. (2005). Axial and radial profiles in conductivities, water storage and native embolism in trunks of young and old-growth ponderosa pine trees. *Plant, Cell & Environment*, *28*, 1103–1113.

Domec, J.-C., Warren, J. M., Meinzer, F. C., & Lachenbruch, B. (2009). Safety factors for xylem failure by implosion and air-seeding within roots, trunks and branches of young and old conifer trees. *IAWA Journal*, *30*, 100–120.

Farquhar, G. D., von Caemmerer, S., & Berry, J. A. (1980). A biochemical model of photosynthetic CO2 assimilation in leaves of C3 species. *Planta*, *149*, 78–90.

Givnish, T. J., Wong, S. C., Stuart-Williams, H., Holloway-Phillips, M., & Farquhar, G. D. (2014). Determinants of maximum tree height in *Eucalyptus* species along a rainfall gradient in Victoria, Australia. *Ecology*, *95*, 2991–3007.

Halle, F., Oldeman, R. A. A., & Tomlinson, P. B. (1978). *Tropical forests and trees: An architectural analysis*. Berlin: Springer-Verlag.

Huber, B. (1928). *Weitere quantitative Untersuchungen über das Wasserleitungssystem der Pflanzen*.

Johnson, D. M., Wortemann, R., McCulloh, K. A., Jordan-Meille, L., Ward, E., Warren, J. M., … Domec, J.-C. (2016). A test of the hydraulic vulnerability segmentation hypothesis in angiosperm and conifer tree species. *Tree Physiology*, *36*, 983–993.

de Jong van Lier, Q., van Dam, J. C., Metselaar, K., de Jong, R., & Duijnisveld, W. H. M. (2008). Macroscopic root water uptake distribution using a matric flux potential approach. *Vadose Zone Journal*, *7*, 1065.

Koch, G. W., Sillett, S. C., Jennings, G. M., & Davis, S. D. (2004). The limits to tree height. *Nature*, *428*, 851–854.

Lawlor, D. W., & Tezara, W. (2009). Causes of decreased photosynthetic rate and metabolic capacity in water-deficient leaf cells: A critical evaluation of mechanisms and integration of processes. *Annals of Botany*, *103*, 561–579.

Lindenmayer, D. B., & Laurance, W. F. (2017). The ecology, distribution, conservation and management of large old trees. *Biological Reviews*, *92*, 1434–1458.

Loranty, M. M., Mackay, D. S., Ewers, B. E., Traver, E., & Kruger, E. L. (2010). Contribution of competition for light to within-species variability in stomatal conductance. *Water Resources Research*, *46*, n/a–n/a.

Lutz, J. A., Larson, A. J., Freund, J. A., Swanson, M. E., & Bible, K. J. (2013). The importance of large-diameter trees to forest structural heterogeneity. *PLoS One*, *8*, e82784.

Lutz, J. A., Larson, A. J., Swanson, M. E., & Freund, J. A. (2012). Ecological importance of large-diameter trees in a temperate mixed-conifer forest. *PLoS One*, *7*, e36131.

Mackay, D. S., Roberts, D. E., Ewers, B. E., Sperry, J. S., McDowell, N. G., & Pockman, W. T. (2015). Interdependence of chronic hydraulic dysfunction and canopy processes can improve integrated models of tree response to drought. *Water Resources Research*, *51*, 6156–6176.

Manzoni, S., Katul, G., & Porporato, A. (2014). A dynamical-system perspective on plant hydraulic failure. *Water Resources Research*, *50*, 5170–5183.

Manzoni, S., Vico, G., Katul, G., Palmroth, S., Jackson, R. B., & Porporato, A. (2013). Hydraulic limits on maximum plant transpiration and the emergence of the safety-efficiency trade-off. *New Phytologist*, *198*, 169–178.

Martin, T. A., Brown, K. J., Kučera, J., Meinzer, F. C., Sprugel, D. G., & Hinckley, T. M. (2001). Control of transpiration in a 220-year-old *Abies amabilis* forest. *Forest Ecology and Management*, *152*, 211–224.

Matheny, A. M., Bohrer, G., Garrity, S. R., Morin, T. H., Howard, C. J., & Vogel, C. S. (2015). Observations of stem water storage in trees of opposing hydraulic strategies. *Ecosphere*, *6*, 1–13.

McCulloh, K. A., Johnson, D. M., Meinzer, F. C., & Woodruff, D. R. (2014). The dynamic pipeline: Hydraulic capacitance and xylem hydraulic safety in four tall conifer species. *Plant, Cell & Environment*, *37*, 1171–1183.

McCulloh, K. A., & Sperry, J. S. (2005). Patterns in hydraulic architecture and their implications for transport efficiency. *Tree Physiology*, *25*, 257–267.

McCulloh, K. A., Sperry, J. S., & Adler, F. R. (2003). Water transport in plants obeys Murray's law. *Nature*, *421*, 939–942.

McDowell, N., Barnard, H., Bond, B., Hinckley, T., Hubbard, R., Ishii, H., … Whitehead, D. (2002). The relationship between tree height and leaf area: Sapwood area ratio. *Oecologia*, *132*, 12–20.

Mencuccini, M., Minunno, F., Salmon, Y., Martínez-Vilalta, J., & Hölttä, T. (2015). Coordination of physiological traits involved in drought-induced mortality of woody plants. *New Phytologist*, *208*, 396–409.

Meunier, F., Couvreur, V., Draye, X., Vanderborght, J., & Javaux, M. (2017a). Towards quantitative root hydraulic phenotyping: Novel mathematical functions to calculate plant-scale hydraulic parameters from root system functional and structural traits. *Journal of Mathematical Biology*, *75*, 1133–1170.

Meunier, F., Couvreur, V., Draye, X., Vanderborght, J., & Javaux, M. (2017b). Water movement through plant roots: Exact solutions of the water flow equation in roots with varying hydraulic properties. *Hydrology and Earth System Sciences*, *21*, 6519–6540.

Meunier, F., Draye, X., Vanderborght, J., Javaux, M., & Couvreur, V. (2017). A hybrid analytical-numerical method for solving water flow equations in root hydraulic architectures. *Applied Mathematical Modelling*, *52*, 648–663.

Mirfenderesgi, G., Bohrer, G., Matheny, A. M., Fatichi, S., de Moraes Frasson, R. P., & Schäfer, K. V. R. (2016). Tree level hydrodynamic approach for resolving aboveground water storage and stomatal conductance and modeling the effects of tree hydraulic strategy. *Journal of Geophysical Research – Biogeosciences*, *121*, 1792–1813.

Mohr, H., & Schopfer, P. (1995). *Plant physiology*. Berlin: Springer-Verlag.

Mueller, R. C., Scudder, C. M., Porter, M. E., Talbot Trotter, R. III, Gehring, C. A., & Whitham, T. G. (2005). Differential tree mortality in response to severe drought: Evidence for long-term vegetation shifts. *Journal of Ecology*, *93*, 1085–1093.

Nepstad, D. C., Tohver, I. M., Ray, D., Moutinho, P., & Cardinot, G. (2007). Mortality of large trees and lianas following experimental drought in an Amazon forest. *Ecology*, *88*, 2259–2269.

Novick, K., Oren, R., Stoy, P., Juang, J. Y., Siqueira, M., & Katul, G. (2009). The relationship between reference canopy conductance and simplified hydraulic architecture. *Advances in Water Resources*, *32*, 809–819.

Olson, M. E., Anfodillo, T., Rosell, J. A., Petit, G., Crivellaro, A., Isnard, S., … Castorena, M. (2014). Universal hydraulics of the flowering plants: Vessel diameter scales with stem length across angiosperm lineages, habits and climates. *Ecology Letters*, *17*, 988–997.

Olson, M. E., & Rosell, J. A. (2013). Vessel diameter–stem diameter scaling across woody angiosperms and the ecological causes of xylem vessel diameter variation. *New Phytologist*, *197*, 1204–1213.

Pammenter, N. W., & van der Willigen, C. (1998). A mathematical and statistical analysis of the curves illustrating vulnerability of xylem to cavitation. *Tree Physiology*, *18*, 589–593.

Petit, G., Pfautsch, S., Anfodillo, T., & Adams, M. A. (2010). The challenge of tree height in *Eucalyptus regnans*: When xylem tapering overcomes hydraulic resistance. *New Phytologist*, *187*, 1146–1153.

Phillips, N., Nagchaudhuri, A., Oren, R., & Katul, G. (1997). Time constant for water transport in loblolly pine trees estimated from time series of evaporative demand and stem sapflow. *Trees*, *11*, 412–419.

Pigliucci, M., & Preston, K. (Eds.) (2004). *Phenotypic integration: Studying the ecology and evolution of complex phenotypes*. Oxford: Oxford University Press.

Prior, L. D., & Bowman, D. M. J. S. (2014). Big eucalypts grow more slowly in a warm climate: Evidence of an interaction between tree size and temperature. *Global Change Biology*, *20*, 2793–2799.

Richards, L. A. (1931). Capillary conduction of liquids through porous mediums. *Journal of Applied Physics*, *1*, 318–333.

Rifai, S. W., Urquiza Mu oz, J. D., Negrón-Juárez, R. I., Ramírez Arévalo, F. R., Tello-Espinoza, R., Vanderwel, M. C., … Bohlman, S. A. (2016). Landscape-scale consequences of differential tree mortality from catastrophic wind disturbance in the Amazon. *Ecological Applications*, *26*, 2225–2237.

Rowland, L., da Costa, A. C., Galbraith, D. R., Oliveira, R. S., Binks, O. J., Oliveira, A. A., … Meir, P. (2015). Death from drought in tropical forests is triggered by hydraulics not carbon starvation. *Nature*, *528*, 119–122.

Ryan, M. G., & Yoder, B. J. (1997). Hydraulic limits to tree height and tree growth. *Bioscience*, *47*, 235–242.

Sack, L., & Holbrook, N. M. (2006). Leaf hydraulics. *Annual Review of Plant Biology*, *57*, 361–381.

Sanderson, J., Whitbread, F. C., & Clarkson, D. T. (1988). Persistent xylem cross-walls reduce the axial hydraulic conductivity in the apical 20 cm of barley seminal root axes: implications for the driving force for water movement. *Plant, Cell & Environment*, *11*, 247–256.

Savage, V. M., Bentley, L. P., Enquist, B. J., Sperry, J. S., Smith, D. D., Reich, P. B., & von Allmen, E. I. (2010). Hydraulic trade-offs and space filling enable better predictions of vascular structure and function in plants. *Proceedings of the National Academy of Sciences*, *107*, 22722–22727.

Scholz, F. G., Bucci, S. J., Goldstein, G., Meinzer, F. C., Franco, A. C., & Miralles-Wilhelm, F. (2007). Biophysical properties and functional significance of stem water storage tissues in neotropical savanna trees. *Plant, Cell & Environment*, *30*, 236–248.

Slik, J. W. F., Paoli, G., McGuire, K., Amaral, I., Barroso, J., Bastian, M., … Zweifel, N. (2013). Large trees drive forest aboveground biomass variation in moist lowland forests across the tropics. *Global Ecology and Biogeography*, *22*, 1261–1271.

Sperry, J. S., Adler, F. R., Campbell, G. S., & Comstock, J. P. (1998). Limitation of plant water use by rhizosphere and xylem conductance: Results from a model. *Plant, Cell & Environment*, *21*, 347–359.

Sperry, J. S., Hacke, U. G., Oren, R., & Comstock, J. P. (2002). Water deficits and hydraulic limits to leaf water supply. *Plant, Cell & Environment*, *25*, 251–263.

Sperry, J. S., Wang, Y., Wolfe, B. T., Mackay, D. S., Anderegg, W. R. L., McDowell, N. G., & Pockman, W. T. (2016). Pragmatic hydraulic theory predicts stomatal responses to climatic water deficits. *New Phytologist*, *212*, 577–589.

Stephenson, N. L., Das, A. J., Condit, R., Russo, S. E., Baker, P. J., Beckman, N. G., … Zavala, M. A. (2014). Rate of tree carbon accumulation increases continuously with tree size. *Nature*, *507*, 90–93.

Tyree, M. T., & Ewers, F. W. (1991). The hydraulic architecture of trees and other woody plants. *New Phytologist*, *119*, 345–360.

Tyree, M. T., & Sperry, J. S. (1988). Do woody plants operate near the point of catastrophic xylem dysfunction caused by dynamic water stress?: Answers from a model. *Plant Physiology*, *88*, 574–580.

Tyree, M. T., & Sperry, J. S. (1989). Vulnerability of xylem to cavitation and embolism. *Annual Review of Plant Physiology and Plant Molecular Biology*, *40*, 19–36.

Wang, H., Prentice, I. C., Keenan, T. F., Davis, T. W., Wright, I. J., Cornwell, W. K., … Peng, C. (2017). Towards a universal model for carbon dioxide uptake by plants. *Nature Plants*, *3*, 734–741.

Warren, C. R., & Adams, M. A. (2000). Water availability and branch length determine $\delta^{13}C$ in foliage of *Pinus pinaster*. *Tree Physiology*, *20*, 637–643.

West, G. B., Brown, J. H., & Enquist, B. J. (1999). A general model for the structure and allometry of plant vascular systems. *Nature*, *400*, 664–667.

Wolf, A., Anderegg, W. R. L., & Pacala, S. W. (2016). Optimal stomatal behavior with competition for water and risk of hydraulic impairment. *Proceedings of the National Academy of Sciences*, *113*, E7222–E7230.

Woodruff, D. R., Bond, B. J., & Meinzer, F. C. (2004). Does turgor limit growth in tall trees? *Plant, Cell & Environment*, *27*, 229–236.

Xu, X., Medvigy, D., Powers, J. S., Becknell, J. M., & Guan, K. (2016). Diversity in plant hydraulic traits explains seasonal and inter-annual variations of vegetation dynamics in seasonally dry tropical forests. *New Phytologist*, *212*, 80–95.

Zaehle, S. (2005). Effect of height on tree hydraulic conductance incompletely compensated by xylem tapering. *Functional Ecology*, *19*, 359–364.

Zar, J. H. (1996). *Biostatistical analysis*. Upper Saddle River, New Jersey: Prentice Hall.

Zhang, Y.-J., Meinzer, F. C., Hao, G.-Y., Scholz, F. G., Bucci, S. J., Takahashi, F. S. C., … Goldstein, G. (2009). Size-dependent mortality in a

neotropical savanna tree: The role of height-related adjustments in hydraulic architecture and carbon allocation. *Plant, Cell & Environment*, *32*, 1456–1466.

Zimmerman, M. H. (1983). *Xylem structure and the ascent of sap* (1st ed.). Berlin Heidelberg: Springer-Verlag.

SUPPORTING INFORMATION

Additional supporting information may be found online in the Supporting Information section at the end of the article.

How to cite this article: Couvreur V, Ledder G, Manzoni S, Way DA, Muller EB, Russo SE. Water transport through tall trees: A vertically explicit, analytical model of xylem hydraulic conductance in stems. *Plant Cell Environ*. 2018;1–19. https://doi.org/10.1111/pce.13322